

# Coherent sets for nonautonomous dynamical systems

Gary Froyland, Simon Lloyd, and Naratip Santitissadeekorn

School of Mathematics and Statistics

University of New South Wales

Sydney, NSW 2052, Australia

February 7, 2020

## Abstract

We describe a mathematical formalism and numerical algorithms for identifying and tracking slowly mixing objects in nonautonomous dynamical systems. In the autonomous setting, such objects are variously known as almost-invariant sets, metastable sets, persistent patterns, or strange eigenmodes, and have proved to be important in a variety of applications. In this current work, we explain how to extend existing autonomous approaches to the nonautonomous setting. We call the new time-dependent slowly mixing objects *coherent sets* as they represent regions of phase space that disperse very slowly and remain coherent. The new methods are illustrated via detailed examples in both discrete and continuous time.

## 1 Introduction

The study of transport and mixing in dynamical systems has received considerable attention in the last two decades; see e.g. [31, 46, 1, 47] for discussions of transport phenomena. In particular, the detection of very slowly mixing objects, known variously as almost-invariant sets, metastable sets, persistent patterns, or strange eigenmodes, has found wide application in fields such as fluid dynamics [34, 30, 35], ocean dynamics [21, 22], astrodynamics [4], and molecular dynamics [9, 41]. A shortcoming of this prior work, based around eigenfunctions of Perron–Frobenius operators (or transfer operators, or evolution operators) is the restriction to autonomous systems or periodically forced systems. In this work, we extend the notions of almost-invariant sets, metastable sets, persistent patterns, and strange eigenmodes to time-dependent *Lagrangian coherent sets*. These coherent sets form a time parameterised family of sets that approximately follow the flow and disperse very slowly; in other words *they stay coherent*. Coherent sets are the natural nonautonomous analogue to almost-invariant sets.

The standard dynamical systems model of transport assumes that the motion of passive particles are completely determined by either an autonomous or a time-dependent vector field. Traditional approaches to understanding transport are based upon the determination of the location of geometric objects such as invariant manifolds. In the autonomous setting, an invariant manifold of one dimension less than the ambient space will form an impenetrable

transport barrier. In the periodically-forced setting, primarily in two-dimensional flows, it has been shown that slow mixing in the neighbourhood of invariant manifolds is sometimes controlled by “lobe dynamics” [36, 37, 46]. In the truly non-autonomous, or aperiodically forced setting, finite-time hyperbolic material lines [24] and surfaces [25] have been proposed as generalisations of invariant manifolds that form barriers to mixing. These material lines and surfaces are known as *Lagrangian coherent structures*; see also [42] for an alternative definition. The geometric approach attempts to find co-dimension 1 sets (coherent structures) that form boundaries of coherent sets.

An alternative to the geometric approach is the ergodic theoretic approach, which attempts to locate almost-invariant sets (or metastable sets) directly, rather than inferring their location indirectly from their boundaries. The basic tool is the Perron–Frobenius operator (or transfer operator). Real eigenvalues of this operator close to 1 correspond to eigenmodes that decay at slow (exponential) rates. These eigenmodes are given by the eigenfunctions of the operator corresponding to the large real eigenvalues. Almost-invariant sets are then heuristically determined from these eigenfunctions. Such an approach arose in the context of smooth autonomous maps and flows on subsets of  $\mathbb{R}^d$  [7, 6] about a decade ago. Further theoretical and computational extensions have since been constructed [17, 15, 16]. A parallel series of work specific to time-symmetric Markov processes and applied to identifying molecular conformations was developed in [40, 8, 9] and surveyed in [41].

There have been some recent studies of the connections between slow mixing in *periodically* driven fluid flow and eigenfunctions of Perron–Frobenius operators. Liu and Haller [30] observe via simulation a transient “strange eigenmode” as predicted by classical Floquet theory. Pikovsky and Popovych [34, 35] numerically integrated an advection-diffusion equation to simulate the evolution of a passive scalar, observing that it is the sub-dominant eigenfunction of the Perron–Frobenius operator that describes the most persistent deviation from the unique steady state.

The Perron–Frobenius operator based approach has been successful in a variety of application areas, however, as the key mathematical object is an *eigenfunction*, there is no simple extension of the method to systems that have *nonperiodic* time dependence.

Indeed, Liu and Haller [30] state that:

“...strange eigenmodes may also be viewed as eigenfunctions of an appropriate Frobenius-Perron operator...This fresh approach offers an alternative view on scalar mixing, but leaves the questions of completeness and general time-dependence open.”

It is this question of general time-dependence that we address in the current work. We provide the natural Perron–Frobenius operator framework to handle general time-dependence, state a numerical algorithm, and demonstrate its effectiveness in identifying strange eigenmodes and coherent sets.

An outline of the paper is as follows. In Section 2 we formalise the notions of nonautonomous systems in both discrete and continuous time. In Section 3 we describe a Galerkin projection method that we will use to produce finite matrix representations of Perron–Frobenius operators. In Section 4 we define the critical constructions for the nonautonomous setting. We show that slowly decaying modes are described by the “Oseledets subspaces” or

“Lyapunov vectors” corresponding to compositions of the projected Perron–Frobenius operators. In Section 5 we describe in detail a numerical algorithm to practically compute these slowly decaying modes, and demonstrate that in the continuous time setting, these modes vary continuously in time. Our numerical approach is illustrated firstly in the discrete time setting with an aperiodic composition of interval maps, and secondly in the continuous time setting with an aperiodically forced flow on a cylinder. Section 6 provides some further background on almost-invariant sets and coherent sets and Section 7 describes a new heuristic to extract coherent sets from slowly decaying modes in the nonautonomous setting. This heuristic is then illustrated using the examples from Section 5.

## 2 Nonautonomous Dynamical Systems

We will treat time dependent dynamical systems on a smooth compact  $d$ -dimensional manifold  $M \subset \mathbb{R}^D$ ,  $D \geq d$  in both discrete and continuous time. In order to keep track of “time” we use a probability space  $(\Omega, \mathcal{H}, \mathbb{P})$ , with the passing of time controlled by an ergodic automorphism  $\theta : \Omega \circlearrowleft$ .

### 2.1 Discrete time – Maps

In the discrete time setting, we will think of  $\Omega \subset (\mathbb{Z})^{\mathbb{Z}}$ , and  $\theta$  as a left shift  $\sigma$  on  $\Omega$  defined by  $(\sigma\omega)_i = \omega_{i+1}$ , where  $\omega = (\dots, \omega_{-1}, \omega_0, \omega_1, \dots) \in \Omega$ . We assume that  $(\Omega, \sigma, \mathbb{P})$  is ergodic. Let  $\mathcal{T} = \{T_{\omega_0}\}_{\omega_0 \in \mathbb{Z}}$  be a collection of (possibly non-invertible) piecewise differentiable maps on a compact manifold  $M$ . For brevity, we will sometimes write  $T_\omega$  in place of  $T_{\omega_0}$ . We will define a nonautonomous dynamical system by map compositions of the form  $T_{\sigma^{k-1}\omega} \circ \dots \circ T_{\sigma\omega} \circ T_\omega$ . Define

$$\Phi(k, \omega, x) := \begin{cases} T_{\sigma^{k-1}\omega} \circ \dots \circ T_{\sigma\omega} \circ T_\omega(x), & k > 0; \\ \text{Id}, & k = 0; \\ T_{\sigma^{-k}\omega}^{-1} \circ \dots \circ T_{\sigma^{-2}\omega}^{-1} \circ T_{\sigma^{-1}\omega}^{-1}(x), & k < 0. \end{cases}$$

For  $k \geq 0$  (resp.  $k < 0$ ),  $\Phi(k, \omega, x)$  represents the forward time (resp. backward time)  $k$ -fold application of the nonautonomous dynamics to the point  $x$  initialised at “time”  $\omega$ . Whenever  $T_\omega$  is non-invertible,  $T_\omega^{-1}(x)$  will represent the finite set of all preimages of  $x$ . We call  $\Phi$  a *map cocycle*.

**Definition 1.** Endow  $M$  with the Borel  $\sigma$ -algebra and let  $\mu$  be a probability measure on  $M$ . We call  $\mu$  an *invariant measure* if  $\mu \circ \Phi(-1, \omega, \cdot) = \mu$  for all  $\omega \in \Omega$ .

This definition of an invariant measure is stricter than is usual for random or nonautonomous dynamical systems (eg. Definition 1.4.1 [2]). More generally, one may allow  $\mu = \mu_\omega$  and insist that  $\mu_{\sigma^{-1}\omega} \circ \Phi(-1, \omega, \cdot) = \mu_\omega$  for all  $\omega \in \Omega$ .

**Example 1.** We construct a map cocycle  $\Phi$  by the composition of maps  $T_i$  from a collection  $\mathcal{T}$  according to sequences of indices  $\omega \in \Omega$ . The collection  $\mathcal{T} := \{T_1, T_2, T_3, T_4\}$  consists of expanding maps of the circle  $S^1$ , which we think of as  $[0, 1]$  with endpoints identified. The sequence space  $\Omega \subset \{1, 2, 3, 4\}^{\mathbb{Z}}$  is given by

$$\Omega = \left\{ \omega \in \{1, 2, 3, 4\}^{\mathbb{Z}} : \forall i \in \mathbb{Z}, M_{\omega_i \omega_{i+1}} = 1 \right\},$$

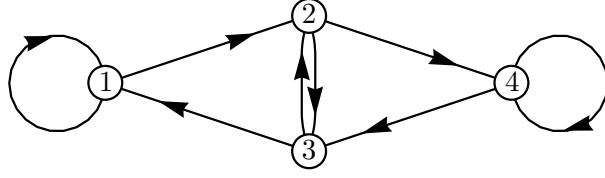


Figure 1: Graph of the sequence space  $\Omega$ .

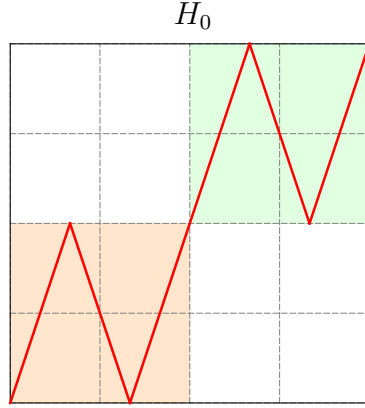


Figure 2: The map  $H_0$  has invariant sets  $[0, 0.5]$  and  $[0.5, 1]$ ; that is,  $H_0^{-1}([0, 0.5]) = [0, 0.5]$  and  $H_0^{-1}([0.5, 1]) = [0.5, 1]$ .

with adjacency matrix

$$M = \begin{pmatrix} 1 & 1 & 0 & 0 \\ 0 & 0 & 1 & 1 \\ 1 & 1 & 0 & 0 \\ 0 & 0 & 1 & 1 \end{pmatrix}.$$

Elements of  $\Omega$  correspond to bi-infinite paths in the graph Figure 1. The shift  $\sigma : \Omega \rightarrow \Omega$  is a subshift of finite type. A Borel  $\sigma$ -algebra  $\mathcal{H}$  is generated by the length-one cylinder sets  $C_i = \{\omega : \omega_0 = i\}$ ,  $i = 1, \dots, 4$ , and by giving equal measure to these four cylinder sets, we generate a shift-invariant probability measure  $\mathbb{P}$ .

The maps of  $\mathcal{T}$  are defined in terms of a continuous piecewise-linear map  $H_a : S^1 \rightarrow S^1$ , which has almost invariant sets (see Definition 5, Section 6)  $[0, 0.5]$  and  $[0.5, 1]$  for a close to zero. Define

$$H_a(x) = \begin{cases} +3x & 0 \leq x < \frac{1}{6} + \frac{1}{2}a, \\ -3x + 3a + 1 & \frac{1}{6} + \frac{1}{2}a \leq x < \frac{1}{3} + \frac{1}{2}a, \\ +3x - a - 1 & \frac{1}{3} + \frac{1}{2}a \leq x < \frac{2}{3} + \frac{1}{2}a, \\ -3x + 3a + 3 & \frac{2}{3} + \frac{1}{2}a \leq x < \frac{5}{6} + \frac{1}{2}a, \\ +3x - 2 & \frac{5}{6} + \frac{1}{2}a \leq x \leq 1, \end{cases}$$

where values are taken modulo 1. Figure 2 shows a graph of  $H_0$ . Let  $a_i \in \mathbb{R}$ ,  $i = 1, \dots, 4$ , be close to zero, for example  $(a_1, a_2, a_3, a_4) = (\pi, 2\sqrt{2}, \sqrt{3}, e)/40$ . We now construct the map

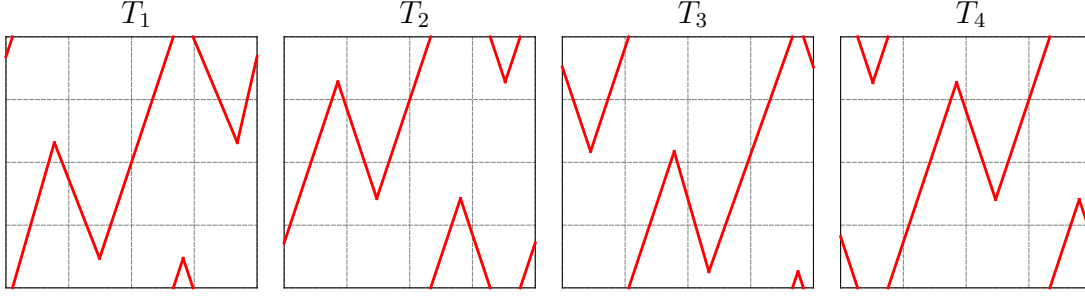


Figure 3: Graphs of  $T_i$  for  $i = 1, \dots, 4$ .

$T_i$  from  $H_{a_i}$ , for  $i = 1, \dots, 4$  as follows:

$$\begin{aligned} T_1 &= H_{a_1}(x) \\ T_2 &= R \circ H_{a_2}(x) \\ T_3 &= H_{a_3} \circ R^{-1} \\ T_4 &= R \circ H_{a_4} \circ R^{-1}, \end{aligned}$$

where  $R : S^1 \rightarrow S^1$  is the rotation  $R(x) = x + 1/4 \pmod{1}$ ; see Figure 3.

Let  $m$  denote normalised Lebesgue measure on  $M$ . To each map  $T_\omega$  we associate a Perron–Frobenius operator  $\mathcal{P}_\omega : L^1(M, m) \rightarrow L^1(M, m)$  defined by  $\mathcal{P}_\omega f = \sum_{y \in T_\omega^{-1}x} f(y) / |\det DT_\omega(y)|$ . The operator  $\mathcal{P}_\omega$  is a linear operator that acts on integrable functions in analogy to the action of  $T_\omega$  on points. If  $f \in L^1(M, m)$  represents a density function for an ensemble of initial conditions, then  $\mathcal{P}_\omega f$  represents the density function of the ensemble after the action of  $T_\omega$  has been applied to the ensemble. The map cocycle  $\Phi$  naturally generates a *Perron–Frobenius cocycle*  $\mathcal{P}_\omega^{(k)} = \mathcal{P}_{\sigma^{k-1}\omega} \circ \dots \circ \mathcal{P}_{\sigma\omega} \circ \mathcal{P}_\omega$ . This composition of  $k$  Perron–Frobenius operators capture the action on a function  $f$  after  $k$  iterations of the non-autonomous system.

## 2.2 Continuous time – Flows

Let  $F : \Omega \times M \rightarrow \mathbb{R}^d$  be a sufficiently regular vector field. More precisely, we suppose that  $F$  satisfies the conditions of Theorem 2.2.2 [2], which will guarantee the existence of a classical solution of the nonautonomous ODE  $\dot{x}(t) = F(\theta^t\omega, x(t))$ ,  $t \in \mathbb{R}$ .

To be concrete about the probability space  $(\Omega, \mathcal{F}, \mathbb{P})$  in the continuous time setting, we may set  $\Omega = \Xi \subset \mathbb{R}^{d_1}$ ,  $d_1 \geq 3$ , and consider an autonomous ODE  $\dot{z} = g(z)$  on  $\Xi$ . Denote the flow for this ODE by  $\xi : \mathbb{R} \times \Xi \rightarrow \Xi$  and suppose that  $\xi$  preserves the probability measure  $\mathbb{P}$ ; that is,  $\mathbb{P} \circ \xi(-t, \cdot) = \mathbb{P}$  for all  $t \in \mathbb{R}$ . Thus, the autonomous, aperiodic flow  $\xi$  drives the nonautonomous ODE

$$\dot{x}(t) = F(\theta^t\omega, x(t)) = F(\xi(t, z), x(t)). \quad (1)$$

We think of points  $z \in \Xi$  as representing generalised time. We assume that  $(\Xi, \xi, \mathbb{P})$  is ergodic in the sense that if  $\xi(-t, \tilde{\Xi}) = \tilde{\Xi}$  for some  $\tilde{\Xi} \subset \Xi$  and for all  $t \geq 0$  then  $\mathbb{P}(\tilde{\Xi}) = 0$  or 1.

**Remark 1.** It is common to simply write  $\dot{x}(t) = F(t, x(t))$ , where  $t \in \mathbb{R}$  is a scalar representing time. However, in order to do ergodic theory we require a driving system leaving

some probability measure  $\mathbb{P}$  invariant. This is not possible if  $\Omega = \mathbb{R}$  and  $\theta^s(t) = t + s$  is a translation by  $s$ . For the formal statements we shall therefore use generalised time  $z \in \Xi$ . In practice, however, one necessarily computes over finite periods of time and so when describing our numerical algorithms and numerical experiments for continuous time we revert to scalar time.

Denote by  $\phi : \mathbb{R} \times \Xi \times M \rightarrow M$  the flow for (1). The flow  $\phi$  satisfies  $\frac{d}{dt}\phi(t, z, x) = F(\xi(t, z), \phi(t, z, x))$ .

**Definition 2.** Endow  $M$  with the Borel  $\sigma$ -algebra and let  $\mu$  be a probability measure on  $M$ . We call  $\mu$  an *invariant measure* if  $\mu \circ \phi(-t, z, \cdot) = \mu$  for all  $z \in \Xi$  and  $t \in \mathbb{R}$ .

**Remark 2.** In Definition 2 we are insisting that  $\mu$  is preserved at all “time instants”. As in the discrete time setting, more generally one may allow  $\mu = \mu_z$  and insist that  $\mu_{\xi(-t, z)} \circ \phi(-t, z, \cdot) = \mu_z$ . However, as we will soon begin to focus on coherent sets rather than invariant measures, we will restrict the invariant measure to a “time independent” measure for clarity of presentation. This is perfectly reasonable for one of the main applications we have in mind, namely, aperiodically driven fluid flow where  $\mu \equiv$  Lebesgue, and volume is preserved by the flow at all times.

**Example 2.** Consider the following nonautonomous system on a cylinder  $M = S^1 \times [0, \pi]$ . Let  $\xi : \mathbb{R} \times \mathbb{R}^3 \rightarrow \mathbb{R}^3$  denote the flow for the driving system generated by the Lorenz system of ODEs (2)–(4) with standard parameters  $\sigma = 10$ ,  $\beta = 8/3$ ,  $\rho = 28$ .

$$\dot{z}_1 = \sigma(z_2 - z_1) \tag{2}$$

$$\dot{z}_2 = \rho z_1 - z_2 - z_1 z_3 / \tau \tag{3}$$

$$\dot{z}_3 = -\beta z_3 + z_1 z_2 / \tau. \tag{4}$$

It is well known that this Lorenz flow possesses an SBR measure  $\mathbb{P}$  [44]. Let the time-dependent vector field  $F : \mathbb{R} \times S^1 \times [0, \pi] \rightarrow S^1 \times [0, \pi]$  generate our non-autonomous flow,  $(\dot{x}(t), \dot{y}(t)) = F(\xi(t, z), x(t), y(t))$ . Explicitly,

$$\dot{x} = c - A \sin(x - \nu z_1(t)) \cos(y) \quad \text{mod } 2\pi \tag{5}$$

$$\dot{y} = A \cos(x - \nu z_1(t)) \sin(y), \tag{6}$$

with  $c = 0.5$ ,  $A = 1$ ,  $\nu = 0.25$ . We take the  $z_1$ -coordinate of the Lorenz driving system to represent the generalized time for the vector field  $F(t, x(t), y(t))$ . We use a scaling factor of  $\tau = 4$  so that the temporal and spatial variation of  $z_1(t)$  is similar to that of the “actual” time  $t$ . Since  $F(z_1(t), x, y)$  is differentiable and bounded on  $M$  for all  $t$ , classical solutions of the nonautonomous ODE (5)–(6) exist. The system (2)–(6) uniquely generates an RDS, see Theorem 2.2.2 in [2]. In Figure 4 we demonstrate a trajectory of three different initial points.

We may define a family of Perron–Frobenius operators as  $\mathcal{P}_z^{(t)} f(x) = f(\phi(-t, \xi(t, z), x)) \cdot |\det D\phi(-t, \xi(t, z), x)|$  for  $t \geq 0$ . This family is a semigroup in  $t$  as  $\mathcal{P}_z^{(t_1+t_2)} f = \mathcal{P}_{\xi(t_1, z)}^{(t_2)} \mathcal{P}_z^{(t_1)} f$ .

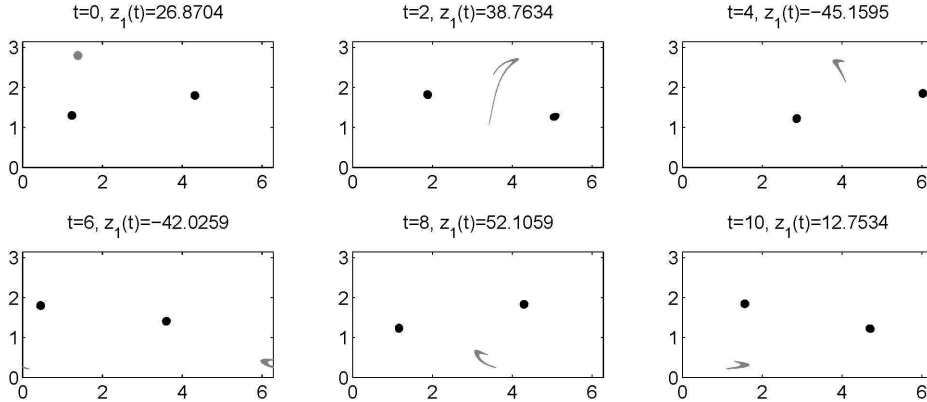


Figure 4: Trajectory of the time-dependent system (5)–(6) driven by the Lorenz system at generalized times  $z_1(t)$

### 3 Galerkin projection and matrix cocycles

Let  $\mathcal{B}_n = \text{sp}\{\chi_{B_i} : B_i \in \mathfrak{B}\}$  where  $\mathfrak{B} = \{B_1, \dots, B_n\}$  is a partition of  $M$  into connected sets of positive Lebesgue measure. Define a projection  $\pi_n : L^1(M, m) \rightarrow \mathcal{B}_n$  as

$$\pi_n f = \sum_{i=1}^n \frac{\int_{B_i} f \, dm}{m(B_i)} \chi_{B_i}. \quad (7)$$

Following Ulam [45], in the sequel we will consider the finite rank operators  $\pi_n \mathcal{P}_\omega^{(1)} : L^1(M, m) \rightarrow \mathcal{B}_n$  and  $\pi_n \mathcal{P}_z^{(1)} : L^1(M, m) \rightarrow \mathcal{B}_n$ , and the matrix representations of the restrictions of  $\pi_n \mathcal{P}_\omega^{(1)}$  and  $\pi_n \mathcal{P}_z^{(1)}$  to  $\mathcal{B}_n$ . We denote these matrix representations (under multiplication on the right) by  $P(\omega)$  and  $P(z)$ . Extending Lemma 2.3 [29] in a straightforward way to the nonautonomous setting, one has

$$P(\omega)_{ij} = \frac{m(B_j \cap \Phi(-1, \sigma\omega, B_i))}{m(B_i)} \quad (8)$$

and

$$P(z)_{ij} = \frac{m(B_j \cap \phi(-1, \xi(1, z), B_i))}{m(B_i)} \quad (9)$$

In particular, these matrices are numerically accessible.

**Remark 3.** Note we do not concern ourselves at all with the relationship between  $\mathcal{P}_\omega^{(1)}$  and  $\pi_n \mathcal{P}_\omega^{(1)}$ ; this is a subtle relationship and beyond the scope of this work. See [29, 13, 10, 32, 14, 3] for work in this direction.

The matrices  $P(\omega)$  and  $P(z)$  generate matrix cocycles

$$P^{(k)}(\omega) := P(\sigma^{k-1}\omega) \cdots P(\sigma\omega) \cdot P(\omega) \quad (10)$$

and

$$P^{(k)}(z) := P(\xi(k-1, z)) \cdots P(\xi(1, z)) \cdot P(z). \quad (11)$$

## 4 Discretised Oseledets functions and the Multiplicative Ergodic Theorem

In periodically driven flows, Liu and Haller [30] and Pikovsky and Popovych [34], observed that certain tracer patterns persisted for long times before eventually relaxing to the equilibrium tracer distribution. Pikovsky and Popovych [34] recognised these patterns as graphs of eigenfunctions of a Perron-Frobenius operator corresponding to an eigenvalue  $L < 1$ . These eigenfunctions decay over time and the closer  $L$  is to 1, the slower the decay and the more slowly an initial tracer distribution will relax to equilibrium. We now develop a framework for the considerably more difficult aperiodic setting.

Consider some suitable Banach space  $(\mathcal{F}, \|\cdot\|)$  of real valued functions;  $\mathcal{F}$  is the function class in which we search for slowly decaying functions. Suppose that the norm is chosen so that for each  $\omega \in \Omega$  and  $k \geq 0$ , the operator  $\mathcal{P}_\omega^{(k)}$  is Markov; that is,  $\|\mathcal{P}_\omega^{(k)}\| = 1$  for all  $\omega$  and  $k \geq 0$ . For  $f \in \mathcal{F}$ , we calculate the following limit:

$$\lambda(\omega, f) = \limsup_{k \rightarrow \infty} \frac{1}{k} \log \|\mathcal{P}_\omega^{(k)} f\|. \quad (12)$$

We refer to  $\lambda(\omega, f) \leq 0$  as the *Lyapunov exponent* of  $f$ . If  $f$  decays under the action of the Perron-Frobenius operators at a geometric rate of  $r^k$ ,  $0 < r < 1$ , then  $\lambda(\omega, f) = \log r$ . The closer  $r$  is to 1, the slower the decay. The extreme case of  $r = 1$  (no decay) is exhibited when  $f$  is the density of the invariant measure  $\mu$  that is common to all maps in our nonautonomous dynamical system. We define the *Lyapunov spectrum*  $\Lambda(\mathcal{P}, \omega) := \{\lambda(\omega, f) : f \in \mathcal{F}\}$ . In the aperiodic setting the new mathematical objects that are analogous to strange eigenmodes and persistent patterns will be called *Oseledets functions*.

**Definition 3.** *Oseledets functions* correspond to  $f$  for which (i)  $\lambda(\omega, f)$  is near zero and (ii) the value  $\lambda(\omega, f)$  is an isolated point in the *Lyapunov spectrum*.

By considering  $(\mathcal{F}, \|\cdot\|) = (\mathcal{B}_n, \|\cdot\|_1)$ , the actions of  $\mathcal{P}_\omega^{(k)}$  and  $\mathcal{P}_z^{(k)}$  are described by  $P^{(k)}(\omega)$  and  $P^{(k)}(z)$ , respectively. We may replace  $\mathcal{P}_\omega^{(k)}$  and  $\mathcal{P}_z^{(k)}$  in (12) by  $P^{(k)}(\omega)$  and  $P^{(k)}(z)$ , respectively, to obtain a standard setting where the possible values of  $\lambda(\omega, f)$  are the Lyapunov exponents of cocycles of  $n \times n$  matrices, and

$$\Lambda(P, \omega) := \left\{ \lim_{k \rightarrow \infty} \frac{1}{k} \log \|P^{(k)}(\omega) f\|_1 : f \in \mathcal{B}_n \right\} \quad (13)$$

and

$$\Lambda(P, z) := \left\{ \lim_{k \rightarrow \infty} \frac{1}{k} \log \|P^{(k)}(z) f\|_1 : f \in \mathcal{B}_n \right\}, \quad (14)$$

exist for  $\mathbb{P}$  almost-all  $\omega \in \Omega$ , and consist of at most  $n$  isolated points,  $\lambda_n < \dots < \lambda_1 = 0$ . Of particular interest to us is the function  $f_2(\omega)$  (or  $f_2(z)$ ) in  $\mathcal{B}_n$ , which represents the function that decays at the slowest possible geometric rate  $\lambda_2$ .

**Remark 4.** In certain settings, this matrix cocycle *exactly* captures all large isolated Lyapunov exponents of the operator cocycle  $\mathcal{P} : (\text{BV}, \|\cdot\|_{\text{BV}}) \circlearrowleft$ . One such setting is a map cocycle formed by composition of piecewise linear expanding maps with a common Markov partition  $\mathfrak{B} = \{B_1, \dots, B_n\}$ ; see [19].

The following example illustrates the concept of Lyapunov spectrum and Oseledets functions in the familiar autonomous setting. For the remainder of this section, we adopt the discrete time notation of  $\sigma$  and  $\omega$ .

**Example 3** (“Autonomous” Single Map). *In [5] individual maps are constructed for which the Perron–Frobenius operator has at least one non-unit isolated eigenvalue when acting on the Banach space  $(BV, \|\cdot\|_{BV})$ . A single autonomous map may be regarded as a cocycle over a one-point space  $\Omega = \{\omega\}$ , and so we may drop the dependence on  $\omega$  in notation. Keller [27] shows that for a piecewise expanding map  $T$  of the interval  $I$ , the spectrum of the associated Perron–Frobenius operator  $\mathcal{P}$  has an essential spectral radius  $\rho(\mathcal{P})$  equal to the asymptotic expansivity  $\sup_{x \in I} \lim_{k \rightarrow \infty} |1/DT^k(x)|^{1/k}$ , and that there are at most countably many spectral points, each isolated, of modulus greater than  $\rho(\mathcal{P})$ . In order to have an isolated spectral point, we construct a map of  $S^1$  which has an almost-invariant set (see Definition 5). The relation between almost-invariant sets and isolated eigenvalues was noted in [7]. Consider the partition  $\mathfrak{B} = \{B_i : i = 1, \dots, 6\}$ , where  $B_i = ((i-1)/6, i/6)$ . Given  $a \in \mathbb{Z}^6$ , any map  $T : S^1 \rightarrow S^1$  defined by*

$$T(x) = 3x - (i-1)/2 + a_i/6 \pmod{1}, \quad x \in B_i \quad (15)$$

is Markov with respect to  $\mathfrak{B}$ . Here we take  $a = (0, 0, 1, 4, 3, 3)$ ; see Figure 5. Notice that there is a low transfer of mass between the two intervals  $[0, 1/2]$  and  $[1/2, 1]$ . Since  $\mathfrak{B}$  is a Markov partition for  $T$ , the space of characteristic functions  $\mathcal{B}_6 = \{\chi_{B_i} : i = 1, \dots, 6\}$  is an invariant subspace of BV for the Perron–Frobenius operator  $\mathcal{P}$  of  $T$ . Thus the action of  $\mathcal{P}_\omega = \mathcal{P}$  on  $\mathcal{F} = \mathcal{B}_6$  is represented by the matrix

$$P = P(\omega) = \frac{1}{3} \begin{pmatrix} 1 & 1 & 0 & 1 & 0 & 0 \\ 1 & 1 & 1 & 0 & 0 & 0 \\ 1 & 1 & 1 & 0 & 0 & 0 \\ 0 & 0 & 1 & 0 & 1 & 1 \\ 0 & 0 & 0 & 1 & 1 & 1 \\ 0 & 0 & 0 & 1 & 1 & 1 \end{pmatrix}, \quad (16)$$

which has non-zero eigenvalues  $L_1 = 1, L_2 = (1 + \sqrt{2})/3, L_3 = (1 - \sqrt{2})/3$ . The map  $T$  is piecewise affine with constant slope 3 and so the local expansion rate is  $\vartheta = \log(1/3)$ .

The eigenvalue  $L_2 \approx 0.805$  of  $P$  thus gives rise to an isolated point  $\lambda_2 \approx \log 0.805$  in the Lyapunov spectrum  $\Lambda(\mathcal{P})$ . The corresponding Oseledets function  $f_2$  is given by  $f_2(x) = \sum_{i=1}^6 w_{2,i} \chi_{B_i}(x)$ , where  $w_2$  is the eigenvector of  $P$  corresponding to the eigenvalue  $L_2$ , see Figure 5. Since  $|L_3| \approx 0.138 < 1/3$ , this means that  $\log L_2$  is the unique isolated Lyapunov exponent in  $\Lambda(\mathcal{P})$ . Note that the set  $\{f_2 > 0\}$  corresponds to the set  $[0, 1/2]$ . We will discuss this property further in Section 7.

**Example 4** (Periodic map cocycle). *We construct a periodic map cocycle from a collection of maps with a common Markov partition. The map cocycle is formed by cyclically composing three maps of  $S^1$ . Consider the sequence space  $\Omega = \{\omega \in \{1, 2, 3\}^{\mathbb{Z}} : \forall i \in \mathbb{Z}, M_{\omega_i, \omega_{i+1}} = 1\}$*

where  $M = \begin{pmatrix} 0 & 1 & 0 \\ 0 & 0 & 1 \\ 1 & 0 & 0 \end{pmatrix}$ . We consider  $\mathcal{T} = \{T_j : j = 1, 2, 3\}$ , where  $T_j$  is given by (15)

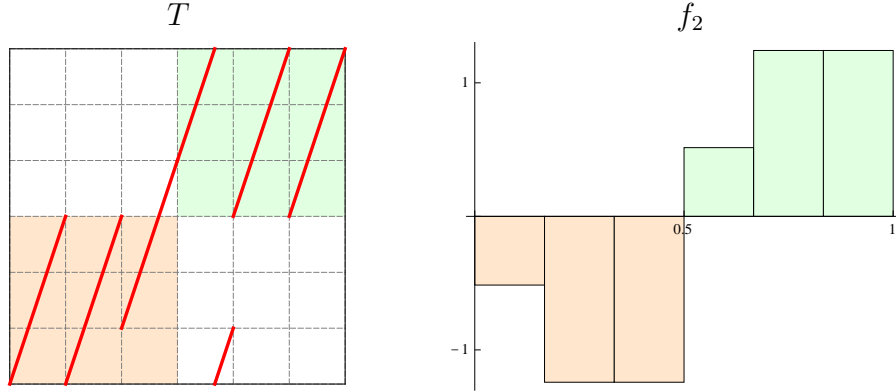


Figure 5: Graph of  $T$  and Oseledets function  $f_2$ .

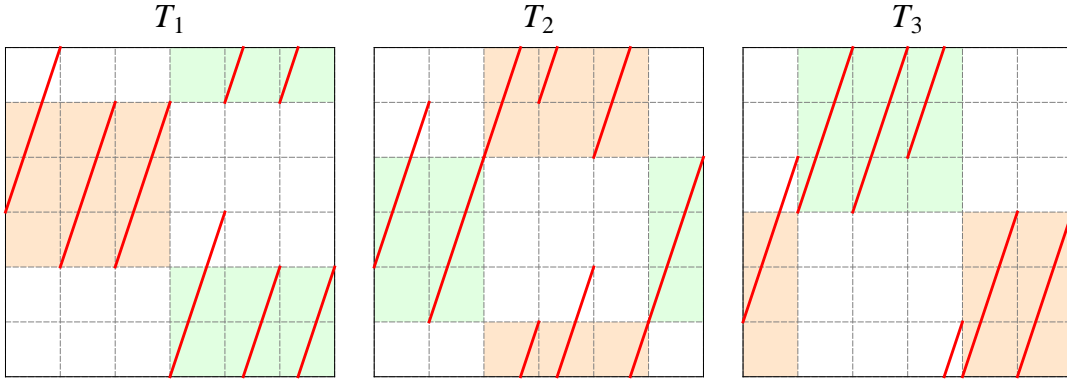


Figure 6: Graphs of  $T_1$ ,  $T_2$  and  $T_3$ .

with parameter  $a^{(j)}$ , where

$$a^{(1)} = (3, 2, 2, 0, 5, 5), \quad a^{(2)} = (2, 1, 4, 5, 4, 1), \quad a^{(3)} = (1, 3, 3, 4, 0, 0),$$

see Figure 6. As in Example 3 we look for Lyapunov exponents that are strictly greater than the log of the long-term local expansion rate of nearby points

$$\rho(\omega) := \sup_{x \in I} \lim_{k \rightarrow \infty} |1/D(T_3 \circ T_2 \circ T_1)^k|^{1/3k}. \quad (17)$$

As each map  $T_j$  is piecewise affine with constant slope 3, the local expansion rate  $\rho(\omega) = 1/3$  and is independent of  $\omega \in \Omega$ . Note also that  $T_1$  approximately maps  $[0, 1/2]$  to  $[1/3, 5/6]$ ,  $T_2$  then maps  $[1/3, 5/6]$  approximately to  $[0, 1/6] \cup [2/3, 1]$ , and finally  $T_3$  maps  $[2/3, 1/3]$  approximately back to  $[0, 1/2]$ . Each map  $T_j$  leaves the space  $\mathcal{B}_6$  from Example 3 invariant, and thus the Perron–Frobenius operator  $\mathcal{P}_j$  of  $T_j$  restricted to  $\mathcal{B}_6$  has matrix representation

$P_j$ , where  $3P_j$ ,  $j = 1, 2, 3$ , are respectively

$$\begin{pmatrix} 0 & 0 & 0 & 1 & 1 & 1 \\ 0 & 0 & 0 & 1 & 1 & 1 \\ 0 & 1 & 1 & 1 & 0 & 0 \\ 1 & 1 & 1 & 0 & 0 & 0 \\ 1 & 1 & 1 & 0 & 0 & 0 \\ 1 & 0 & 0 & 0 & 1 & 1 \end{pmatrix}, \begin{pmatrix} 0 & 0 & 1 & 1 & 1 & 0 \\ 0 & 1 & 0 & 1 & 0 & 1 \\ 1 & 1 & 0 & 0 & 0 & 1 \\ 1 & 1 & 0 & 0 & 0 & 1 \\ 1 & 0 & 1 & 0 & 1 & 0 \\ 0 & 0 & 1 & 1 & 1 & 0 \end{pmatrix}, \begin{pmatrix} 0 & 0 & 0 & 1 & 1 & 1 \\ 1 & 0 & 0 & 0 & 1 & 1 \\ 1 & 0 & 0 & 0 & 1 & 1 \\ 1 & 1 & 1 & 0 & 0 & 0 \\ 0 & 1 & 1 & 1 & 0 & 0 \\ 0 & 1 & 1 & 1 & 0 & 0 \end{pmatrix}. \quad (18)$$

The triple product  $P^{(3)}(\omega) = P_3 P_2 P_1$  has non-zero eigenvalues  $L_1 = 1$ ,  $L_2 = (13 + \sqrt{233})/54$  and  $L_3 = (13 - \sqrt{233})/54$ . Since  $L_2 \approx 0.523$ , its associated eigenvector  $w_2$  satisfies  $\lambda(\omega, w_2) = \log \sqrt[3]{\lambda_2} > \log(1/3)$ . Since  $P^{(3)}(\sigma^k \omega)$ ,  $k = 1, 2$ , are cyclic permutations of the factors of  $P^{(3)}(\omega)$ , they share the same eigenvalues, and in particular  $L_2$ . Thus  $(1/3) \log L_2$  is an isolated Lyapunov exponent of  $\Lambda(\mathcal{P}, \omega)$  for each  $\omega \in \Omega$ . Associated to the eigenvalue  $L_2$ , the matrices  $P(\sigma^k \omega)$ ,  $k = 0, 1, 2$ , have corresponding eigenvectors  $w_2(\sigma^k \omega)$ . The three vectors  $w_2(\sigma^k \omega)$ ,  $k = 0, 1, 2$ , generate the periodic Oseledets functions  $f_2(\sigma^k \omega) = \sum_{i=1}^6 w_{2,i}(\sigma^{k \pmod{3}} \omega) \chi_{B_i}$ , see Figure 7. Note that the sets  $\{f_2(\sigma^k \omega) > 0\}_{k=0,1,2}$  correspond to the sets  $[0, 1/2]$ ,  $[1/3, 5/6]$ ,

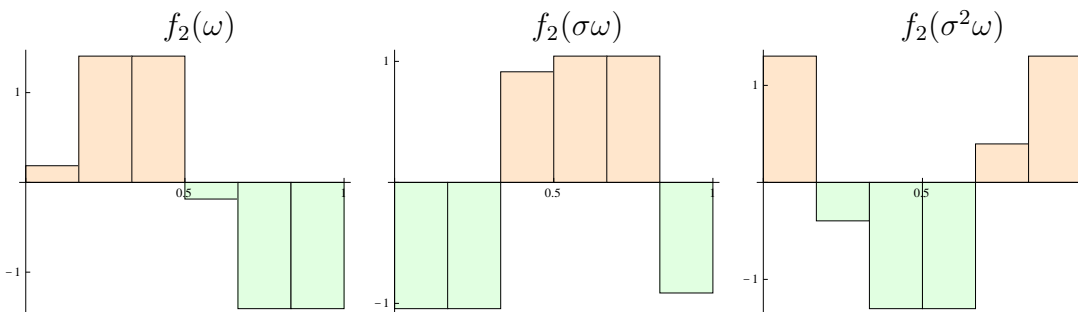


Figure 7: Oseledets functions  $f_2(\sigma^k \omega)$  for  $k = 0, 1, 2$ .

and  $[0, 1/6] \cup [2/3, 1]$ , respectively. We will discuss this property further in Section 7. For another such example see [19]. See also [20] for a detailed example of similar calculations for a periodically driven flow.

In the nonautonomous setting, we can no longer easily construct Oseledets functions as eigenfunctions of a single operator, or eigenvectors of a single matrix. In fact, the Oseledets functions are themselves (aperiodically) time dependent in the nonautonomous setting. Our model of Oseledets functions for nonautonomous systems is, as the name suggests, built around the Multiplicative Ergodic Theorem, see eg. Chapter 3, §4 [2]. We now state a strengthened version [19] of the Multiplicative Ergodic Theorem that we require for our current purposes.

**Theorem 1** ([19]). *Let  $\sigma$  be an invertible ergodic measure-preserving transformation of the space  $(\Omega, \mathcal{H}, \mathbb{P})$ . Let  $P : \Omega \rightarrow M_n(\mathbb{R})$  be a measurable family of matrices satisfying*

$$\int \log^+ \|P(\omega)\| d\mathbb{P}(\omega) < \infty.$$

Then there exist  $\lambda_1 > \lambda_2 > \dots > \lambda_\ell \geq -\infty$  and dimensions  $m_1, \dots, m_\ell$ , with  $m_1 + \dots + m_\ell = n$ , and a measurable family of subspaces  $W_j(\omega) \subseteq \mathbb{R}^n$  such that for almost every  $\omega \in \Omega$  the following hold:

1.  $\dim W_j(\omega) = m_j$ ;
2.  $\mathbb{R}^n = \bigoplus_{j=1}^{\ell} W_j(\omega)$ ;
3.  $P(\omega)W_j(\omega) \subseteq W_j(\sigma\omega)$  (with equality if  $\lambda_j > -\infty$ );
4. for all  $v \in W_j(\omega) \setminus \{0\}$ , one has

$$\lim_{k \rightarrow \infty} (1/k) \log \|P(\sigma^{k-1}\omega) \cdots P(\sigma\omega) \cdot P(\omega)v\| = \lambda_j.$$

The subspaces  $W_j(\omega)$  are the general time-dependent analogues of the vectors  $w_2$  and  $w_2(\sigma^k\omega)$ ,  $k = 0, 1, 2$  of Examples 3 and 4, respectively. We may explicitly construct the slowest decaying discrete Oseledets function as  $f_2(\omega) := \sum_{i=1}^n w_{2,i}(\omega) \chi_{B_i}$ , where  $w_2(\omega) \in W_2(\omega)$ . In the sequel, for brevity we will often call  $W_j(\omega)$  a subspace or a function, recognising its dual roles.

**Remark 5.** We remark that if  $\ell \geq 2$ ,  $m_2 = 1$ , and  $\lambda_2 > -\infty$ , the family of vectors  $\{f_2(\sigma^k\omega)\}_{k \geq 0}$  is the *unique*<sup>1</sup> (up to scalar multiples) family of vectors in  $\mathcal{B}_n$  with the properties that

1.  $\lim_{k' \rightarrow \infty} (1/k') \log \|P^{(k')}(\omega) f_2(\sigma^{k'}\omega)\|_1 = \lambda_2$ ,  $k \geq 0$ ,
2.  $\pi_n \mathcal{P}_\omega f_2(\sigma^k\omega) = \alpha_k f_2(\sigma^{k+1}\omega)$  for some  $\alpha_k \neq 0$ ,  $k \geq 0$ .

**Remark 6.** Theorem 1 strengthens the standard version of the MET for one-sided time with noninvertible matrices (see eg. Theorem 3.4.1 [2]) to obtain the conclusions of the two-sided time MET with invertible matrices (see eg. Theorem 3.4.11 [2]). In Theorem 3.4.1 [2], the existence of only a *flag*  $\mathbb{R}^n = V_1(\omega) \supset \dots \supset V_\ell(\omega)$  of Oseledets subspaces is guaranteed, while in Theorem 3.4.11 [2], the existence of a *splitting*  $W_1(\omega) \oplus \dots \oplus W_\ell(\omega) = \mathbb{R}^n$  is guaranteed. Theorem 1 above demonstrates existence of an Oseledets *splitting* for two-sided time with *noninvertible* matrices. This is particularly important for our intended application as the projected Perron–Frobenius operator matrices are non-invertible.

## 5 Numerical approximation of Oseledets functions

In the autonomous and periodic settings we have seen in Examples 3 and 4 that the subspaces  $W_2(\omega) = \text{sp}\{w_2(\omega)\}$  were one-dimensional, and that the vectors  $w_2(\omega)$  could be simply determined as eigenvectors of matrices. For truly nonautonomous systems (those that are aperiodically driven), the Oseledets splittings are difficult to compute. In this section we outline a numerical algorithm to approximate the  $W_j(\omega)$  subspaces from Theorem 1. The algorithm is based on the push-forward limit argument developed in the proof of Theorem 1. To streamline notation, we describe the discrete time and continuous time setting separately.

---

<sup>1</sup>Assume there is another family  $\{w'_2(\sigma^k\omega)\}_{k \geq 0} \neq \{w_2(\sigma^k\omega)\}_{k \geq 0}$  (up to scalar multiples) with these properties. Then  $w'_2(\sigma^k\omega) = \sum_{j=2}^{\ell} \alpha_{k,j} w_j(\sigma^k\omega)$  for some  $\alpha_{k,j}$ ,  $j = 2, \dots, \ell$ , with  $\alpha_{k,2} \neq 0$ . WLOG assume  $\alpha_{k,2}, \alpha_{k,j'} \neq 0$  for some  $2 < j' \leq \ell$  and all  $k \geq 0$ , but that  $\alpha_{k,j} = 0$  for all  $j \neq 2, j'$  and all  $k \geq 0$ . Then  $m_2 \geq 2$  in Theorem 1, a contradiction.

## 5.1 Discrete time

We first describe a simple and efficient method to construct the matrix  $P(\omega)$  defined in (8).

**Algorithm 1** (Approximation of  $P(\sigma^{-k}\omega)_{ij}$ ,  $0 \leq k \leq N$ ).

1. Partition the state space  $M$  into a collection of connected sets  $\{B_1, \dots, B_n\}$  of small diameter.
2. Fix  $i, j$ , and  $k$  and create a set of  $Q$  test points  $x_{j,1}, \dots, x_{j,Q} \in B_j$  that are uniformly distributed over  $B_j$ .
3. For each  $q = 1, \dots, Q$  calculate  $y_{j,q} = T_{\sigma^{-k}\omega} x_{j,q}$ .
4. Set

$$P(\sigma^{-k}\omega)_{ij} = \frac{\#\{q : y_{j,q} \in B_i\}}{Q} \quad (19)$$

We now describe how to use the matrices  $P(\omega)$  to approximate the subspaces  $W_j(\omega)$ . An intuitive description of the ideas behind Algorithm 2 immediately follows the algorithm statement.

**Algorithm 2** (Approximation of Oseledets subspaces  $W_j(\omega)$  at  $\omega \in \Omega$ ).

1. Construct the Ulam matrices  $P^{(M)}(\sigma^{-N}\omega)$  and  $P^{(N)}(\sigma^{-N}\omega)$  from (19) and (10) for suitable  $M$  and  $N$ . The number  $M$  represents the number of iterates over which one measures the decay, while the number  $N$  represents how many iterates the resulting “initial vectors” are pushed forward to better approximate elements of the  $W_j(\omega)$ .

2. Form

$$\Psi^{(M)}(\sigma^{-N}\omega) := (P^{(M)}(\sigma^{-N}\omega)^\top P^{(M)}(\sigma^{-N}\omega))^{1/2M}$$

as an approximation to the standard limiting matrix

$$B(\sigma^{-N}\omega) := \lim_{M \rightarrow \infty} (P^{(M)}(\sigma^{-N}\omega)^\top P^{(M)}(\sigma^{-N}\omega))^{1/2M}$$

appearing in the Multiplicative Ergodic Theorem (see eg. Theorem 3.4.1(i) [2]).

3. Calculate the orthonormal eigenspace decomposition of  $\Psi^{(M)}(\sigma^{-N}\omega)$ , denoted by  $U_j^{(M)}(\sigma^{-N}\omega)$ ,  $j = 1, \dots, \ell$ . We are particularly interested in low values of  $j$ , corresponding to large eigenvalues  $L_j$ .
4. Define  $W_j^{(M,N)}(\omega) := P^{(N)}(\sigma^{-N}\omega)U_j^{(M)}(\sigma^{-N}\omega)$  via the push forward under the matrix cocycle.
5.  $W_j^{(M,N)}(\omega)$  is our numerical approximation to  $W_j(\omega)$ .

Here is the idea behind the above algorithm. If we choose  $M$  large enough, the eigenspace  $U_j^{(M)}(\sigma^{-N}\omega)$  should be close to the limiting ( $M \rightarrow \infty$ ) eigenspace  $U_j(\sigma^{-N}\omega)$ . Vectors in the eigenspace  $U_j(\sigma^{-N}\omega)$  experience stretching at a rate close to  $L_j$ . Note that the eigenspace  $U_j^{(M)}(\sigma^{-N}\omega)$  is the  $j^{\text{th}}$  singular vector of the matrix  $P^{(M)}(\sigma^{-N}\omega)$ , which experiences a “per unit time” average stretching from time  $-N$  to  $-N + M$  of  $L_j$ . Choose some arbitrary  $v \in U_j(\sigma^{-N}\omega)$  and write  $v = \sum_{j'=j}^{\ell} w_{j'}$  with  $w_{j'} \in W_{j'}(\sigma^{-N}\omega)$ . Pushing forward by  $P^{(N)}(\sigma^{-N}\omega)$  for large enough  $N$  will result in  $\|P^{(N)}(\sigma^{-N}\omega)w_j\|$  dominating  $\|P^{(N)}(\sigma^{-N}\omega)w_{j'}\|$  for  $j < j' \leq \ell$ . Thus, for large  $M$  and  $N$  we expect  $W_j^{(M,N)}(\omega)$  to be close to  $W_j(\omega)$ .

**Remarks 1.**

1. Theorem 1 states that  $W_j^{(\infty,N)}(\omega) \rightarrow W_j(\omega)$  as  $N \rightarrow \infty$ .
2. This method may also be used to calculate the Oseledets subspaces for two-sided linear cocycles, and may be more convenient, especially for large  $n$ , than the standard method of intersecting the relevant subspaces of flags of the forward and backward cocycles.

The numerical approximation of the Oseledets subspaces has been considered by a variety of authors in the context of (usually invertible) nonlinear differentiable dynamical systems, where the linear cocycle is generated by Jacobian matrices concatenated along trajectories of the nonlinear system. Froyland *et al.* [18] approximate the Oseledets subspaces in invertible two-dimensional systems by multiplying a randomly chosen vector by  $P^{(N)}(\sigma^{-N}\omega)$  (pushing forward) or  $P^{(-N)}(\sigma^N\omega)$  (pulling back, where  $P^{(-N)}(\sigma^N\omega) = P^{-1}(\omega) \cdots P^{-1}(\sigma^{N-1}\omega)$ ). Trevison and Pancotti [43] calculate eigenvectors of  $\Psi^{(M)}(\omega)$  for the three-dimensional Lorenz flow, increasing  $M$  until numerical convergence of the eigenvectors is observed. Ershov and Potapov [12] use an approach similar to ours, combining eigenvectors of a  $\Psi^{(M)}$  with pushing forward under  $P^{(N)}$ . Ginelli *et al.* [23] embed the approach of [18] in a QR-decomposition methodology to estimate the Oseledets vectors in higher dimensions. In the numerical experiments that follow, we have found our approach to work very well, with fast convergence in terms of both  $M$  and  $N$ .

## 5.2 Continuous time

As our practical computations are necessarily over finite time intervals, from now on, when dealing with continuous time systems, we will

1. Compute  $P^{(k)}(z)$  as  $\pi_n \mathcal{P}_z^{(k)}$  rather than as  $P(\xi(k-1, z)) \cdots P(\xi(1, z)) \cdot P(z)$ . If the computation of  $\pi_n \mathcal{P}_z^{(k)}$  can be done accurately (this will be discussed further in Section 5.5), then this representation should be closer to  $\mathcal{P}_z^{(k)}$  as there are fewer applications of  $\pi_n$ .
2. Replace the “generalised time”  $z \in \Xi$  with scalar time  $t \in \mathbb{R}$ . That is,  $P^{(\tau)}(t) = \pi_n \mathcal{P}_t^{(\tau)}$  will denote the Perron–Frobenius operator describing the nonautonomous flow from time  $t$  for a duration  $\tau$ . This simplification will streamline the notation in the algorithms, proofs, and numerical examples to follow.

We first describe a simple and efficient method to construct the matrix  $P(\omega)$  defined in (8).

**Algorithm 3** (Approximation of  $P^{(M)}(t - N)$ ,  $t \geq 0$ ).

1. Partition the state space  $M$  into a collection of connected sets  $\{B_1, \dots, B_n\}$  of small diameter.
2. Fix  $i, j$ , and  $t$  and create a set of  $Q$  test points  $x_{j,1}, \dots, x_{j,Q} \in B_j$  that are uniformly distributed over  $B_j$ .
3. For each  $q = 1, \dots, Q$  calculate  $y_{j,q} = \phi(M, t - N, x_{j,q})$ .
4. Set

$$P^{(M)}(t - N)_{ij} = \frac{\#\{q : y_{j,q} \in B_i\}}{Q} \quad (20)$$

The flow time  $M$  should be chosen long enough so that most test points leave their partition set of origin, otherwise at the resolution given by the partition  $\{B_1, \dots, B_n\}$ , the matrix  $P^{(M)}(t - N)$  matrix will be too close to the  $n \times n$  identity matrix. If the action of  $\phi$  separates nearby points, as is the case for chaotic systems, clearly the longer the flow duration  $M$ , the greater  $Q$  should be in order to maintain a good representation of the images  $\phi(M, t - N, B_i)$  by the test points.

**Algorithm 4** (Approximation of Oseledets subspaces  $W_j(t)$  at  $t \in \mathbb{R}$ ).

1. Construct the Ulam matrices  $P^{(M)}(t - N)$  and  $P^{(N)}(t - N)$  from (20) for suitable  $M$  and  $N$ . The number  $M$  represents the flow duration over which rate of decay is measured, while the number  $N$  represents the duration over which the resulting “initial vectors” are pushed forward to better approximate elements of the  $W_j(\omega)$ .

2. Form

$$\Psi^{(M)}(t - N) := (P^{(M)}(t - N)^\top P^{(M)}(t - N))^{1/2M}$$

as an approximation to the standard limiting matrix

$$B(t - N) := \lim_{M \rightarrow \infty} (P^{(M)}(t - N)^\top P^{(M)}(t - N))^{1/2M}$$

appearing in the Multiplicative Ergodic Theorem (see eg. Theorem 3.4.1(i) [2]).

3. Calculate the orthonormal eigenspace decomposition of  $\Psi^{(M)}(t - N)$ , denoted by  $U_j^{(M)}(t - N)$ ,  $j = 1, \dots, \ell$ . We are particularly interested in low values of  $j$ , corresponding to large eigenvalues  $L_j$ .
4. Define  $W_j^{(M,N)}(t) := P^{(N)}(t - N)U_j^{(M)}(t - N)$  via the push forward under the matrix cocycle.
5.  $W_j^{(M,N)}(t)$  is our numerical approximation to  $W_j(t)$ .

### 5.3 Continuity of the Oseledets subspaces in continuous time

When treating continuous time systems, one may ask about the continuity properties of  $W_j^{(M,N)}(t)$  in  $t$ . In the following we suppose that  $W_2^{(M,N)}(t)$  is one-dimensional. For large  $M$  and  $N$ ,  $W_2^{(M,N)}(t)$  will approximate the most dominant Oseledets subspace at time  $t$ . Suppose that we are interested in how this subspace changes from time  $t$  to time  $t + \delta$  for small  $\delta > 0$ . There are two ways to obtain information at time  $t + \delta$ . Firstly, we can simply push forward  $W_2^{(M,N)}(t)$  slightly longer to produce  $W_2^{(M,N+\delta)}(t + \delta)$ . Secondly, we can compute  $\Psi^{(M)}$  slightly later at time  $t + \delta$  to produce  $W_2^{(M,N)}(t + \delta)$ .

To compare the closeness of  $W_2^{(M,N)}(t)$  to  $W_2^{(M,N+\delta)}(t + \delta)$  and  $W_2^{(M,N)}(t + \delta)$ , we represent each as a function and make a comparison in the  $L^1$  norm. We assume that  $U_2^{(M)}(t - N)$  is one-dimensional and define  $f_{n,t-N,M} = \sum_{i=1}^n (u_2^{(M)}(t - N))_i \chi_{B_i} \in L^1(M, m)$  where  $u_2^{(M)}(t - N) \in U_2^{(M)}(t - N)$  is scaled so that  $\|f_{n,t-N,M}\|_1 = 1$ . Let  $\hat{f}_{n,t,M,N} = \pi_n \mathcal{P}_{t-N}^{(N)} f_{n,t-N,M}$ . Note that  $\hat{f}_{n,t,M,N} = \sum_{i=1}^n (w_2^{(M,N)}(t))_i \chi_{B_i}$  for some  $w_2^{(M,N)}(t) \in W_2^{(M,N)}(t)$ .

We firstly compare  $\hat{f}_{n,t+\delta,M,N+\delta}$  and  $\hat{f}_{n,t,M,N}$ .

**Proposition 1.**  $\|\hat{f}_{n,t+\delta,M,N+\delta} - \hat{f}_{n,t,M,N}\|_1 \rightarrow 0$  as  $\delta \rightarrow 0$ .

*Proof.* Note that  $\hat{f}_{n,t+\delta,M,N+\delta} = \pi_n \mathcal{P}_{t-N}^{(N+\delta)} f_{n,t-N,M}$  while  $\hat{f}_{n,t,M,N} = \pi_n \mathcal{P}_{t-N}^{(N)} f_{n,t-N,M}$ . The proof will follow from the result that  $\mathcal{P}_z^{(\tau)}$  is a *continuous* semigroup; that is,  $\lim_{\delta \rightarrow 0} \|\mathcal{P}_t^{(\delta)} f - f\|_1 = 0$  for all  $t \in \mathbb{R}$ ,  $f \in L^1(M, m)$ .

**Lemma 1.**  $\|\mathcal{P}_t^{(\delta)} f - f\|_1 \rightarrow 0$  as  $\delta \rightarrow 0$  for all  $t \in \mathbb{R}$  and  $f \in L^1$ .

*Proof.* The proof runs as a non-autonomous version of the discussion in Remark 7.6.2 [28]. Note that  $\mathcal{P}_t^{(\delta)} f(x) = f(\phi(-\delta, t + \delta, x)) \cdot \det D\phi(-\delta, t + \delta, x)$ , where  $\phi(-\delta, t + \delta, \cdot)$  denotes the flow from  $t + \delta$  in reverse time for duration  $\delta$ . For the moment consider continuous  $f$ . Since  $x \mapsto \phi(s, t, x)$  is at least  $C^1$  for each  $s, t$  (the derivative of  $\phi$  wrt to  $x$  is continuous with respect to  $s$  and  $x$  for each fixed  $t$ ) by Theorem 2.2.2 (iv) [2] and  $M$  is compact,  $\mathcal{P}_t^{(\delta)} f(x) \rightarrow f(x)$  uniformly in  $x$  as  $\delta \rightarrow 0$ . Thus  $\|\mathcal{P}_t^{(\delta)} f - f\|_1 \rightarrow 0$  as  $\delta \rightarrow 0$ . Since the continuous functions are dense in  $L^p$ ,  $1 \leq p < \infty$  as  $M$  is compact (see eg. [11] Lemma IV.8.19), one can  $L^1$  approximate any  $L^1$   $f$  by a continuous function and thus the result holds for all  $L^1$  functions  $f$ .  $\square$

Thus the result follows using Lemma 1 and the fact that  $\|\pi_n\|_1 = 1$ .  $\square$

Now, let's compare  $\hat{f}_{n,t+\delta,M,N}$  and  $\hat{f}_{n,t,M,N}$ .

**Proposition 2.**  $\|\hat{f}_{n,t+\delta,M,N} - \hat{f}_{n,t,M,N}\|_1 \rightarrow 0$  as  $\delta \rightarrow 0$ .

*Proof.* This result is more difficult to demonstrate as we need to firstly compare  $\Psi^{(M)}(t - N)$

with  $\Psi^{(M)}(t - N + \delta)$ . To this end, consider

$$\begin{aligned}
\|\pi_n \mathcal{P}_{t-N+\delta}^{(M)} f - \pi_n \mathcal{P}_{t-N}^{(M)} f\|_1 &= \|\pi_n \mathcal{P}_{t+\delta-N}^{(M)} f - \pi_n \mathcal{P}_{t-N}^{(M+\delta)} f + \pi_n \mathcal{P}_{t-N}^{(M+\delta)} f - \pi_n \mathcal{P}_{t-N}^{(M)} f\|_1 \\
&\leq \|\pi_n\|_1 \left( \|\mathcal{P}_{t-N+\delta}^{(M)} f - \mathcal{P}_{t-N}^{(M+\delta)} f\|_1 + \|\mathcal{P}_{t-N}^{(M+\delta)} f - \mathcal{P}_{t-N}^{(M)} f\|_1 \right) \\
&\leq \|\mathcal{P}_{t-N+\delta}^{(M)} (\text{Id} - \mathcal{P}_{t-N}^{(\delta)}) f\|_1 + \|(\mathcal{P}_{t-N+M}^{(\delta)} - \text{Id}) \mathcal{P}_{t-N}^{(M)} f\|_1 \\
&\leq \|(\text{Id} - \mathcal{P}_{t-N}^{(\delta)}) f\|_1 + \|(\mathcal{P}_{t-N+M}^{(\delta)} - \text{Id}) \mathcal{P}_{t-N}^{(M)} f\|_1
\end{aligned}$$

The right hand side converges to zero as  $\delta \rightarrow 0$  by Lemma 1. This result implies that  $\|P^{(M)}(t - N) - P^{(M)}(t - N + \delta)\| \rightarrow 0$  as  $\delta \rightarrow 0$  in whatever matrix norm we choose. Thus  $\|\Psi^{(M)}(t - N)^{2M} - \Psi^{(M)}(t - N + \delta)^{2M}\| = \|P^{(M)}(t - N)^\top (P^{(M)}(t - N) - P^{(M)}(t - N + \delta)) + (P^{(M)}(t - N)^\top - P^{(M)}(t - N + \delta)^\top) P^{(M)}(t - N + \delta)\| \rightarrow 0$  as  $\delta \rightarrow 0$ . By standard perturbation results, see eg. Theorem II.5.1 [26], this implies that eigenvectors  $U_2^{(M)}(t)$  and  $U_2^{(M)}(t + \delta)$  are close for sufficiently small  $\delta$ . Thus  $f_{n,t-N,M}$  and  $f_{n,t-N+\delta,M}$  are close in  $L^1$  norm. Now we need to push both of these forward by  $\pi_n \mathcal{P}(t - N)^{(N)}$ . This will not increase the norm of the difference at all, so  $\|\hat{f}_{n,t+\delta,M,N} - \hat{f}_{n,t,M,N}\|_1$  will also be small.  $\square$

## 5.4 Oseledets functions for a 1D discrete time nonautonomous system

We now examine the Oseledets functions for the system defined in Example 1. We consider the approximation  $\pi_{100} \mathcal{P}_\omega$  of rank 100, which we obtain by Galerkin projection. We denote by  $P(\omega) \in \mathbb{R}^{100} \times \mathbb{R}^{100}$  the Ulam matrix representing the action of  $\pi_{100} \mathcal{P}_\omega$  on functions  $f \in \mathcal{B}_{100} := \text{sp}\{\chi_{[(i-1)/100, i/100)}, i = 1, \dots, 100\}$ . The matrices  $P(\sigma^{-k}\omega)$ ,  $k = -10, \dots, 10$  are constructed by following Algorithm 1 using  $Q = 100$ .

We look for Oseledets functions for a particular aperiodic sequence  $\omega$ . To generate an aperiodic sequence, let  $\tau \in \{0, 1\}^{\mathbb{N}}$  be the binary expansion of  $1/\sqrt{3}$ . Extend  $\tau$  to an element of  $\{0, 1\}^{\mathbb{Z}}$  by setting  $\tau_i = 0$  for all  $i \leq 0$ . Define  $\omega_{i-25} = 1 + 2\tau_i + \tau_{i+1}$  for each  $i$ . Then  $\omega \in \Omega$  and the central 21 terms of  $\omega$  are

$$\omega = (\dots, 2, 3, 1, 2, 4, 4, 3, 2, 3, 1, \dot{1}, 2, 3, 2, 4, 3, 1, 2, 3, 1, 1\dots), \quad (21)$$

where the dot denotes the zeroth term  $\omega_0 = 1$ .

We calculate the eigenvalues of  $(P^{(20)}(\sigma^{-10}\omega)^\top \circ P^{(20)}(\sigma^{-10}\omega))^{1/40}$ , where  $P^{(20)}(\sigma^{-10}\omega)$  is defined as in (10), and find the top three to be

$$L_1 \approx 1.00, L_2 \approx 0.84, L_3 \approx 0.46.$$

As in Examples 3 and 4, the maps  $T_i$  are piecewise affine with constant slope three, and so  $\rho(\omega) = 1/3$ . Thus  $\log L_2$  and  $\log L_3$  may approximate isolated Lyapunov exponents in  $\Lambda(\mathcal{P})$ .

We follow Algorithm 2 to approximate the second Oseledets subspace  $W_2^{(M,N)}(\sigma^k\omega)$  for  $k = 0, \dots, 5$ , using  $(M, N) = (20, 10)$ , see Figure 8. In order to confirm the effectiveness of Algorithm 2 we calculate the  $L^1$  distance  $\Delta(N)$  between the normalisations of the vectors  $w_2^{(2N,N)}(\sigma\omega)$  and  $P(\omega)w_2^{(2N,N)}(\omega)$ , for  $N = 2, \dots, 19$  with  $M = 40$ . By property 3 of Theorem

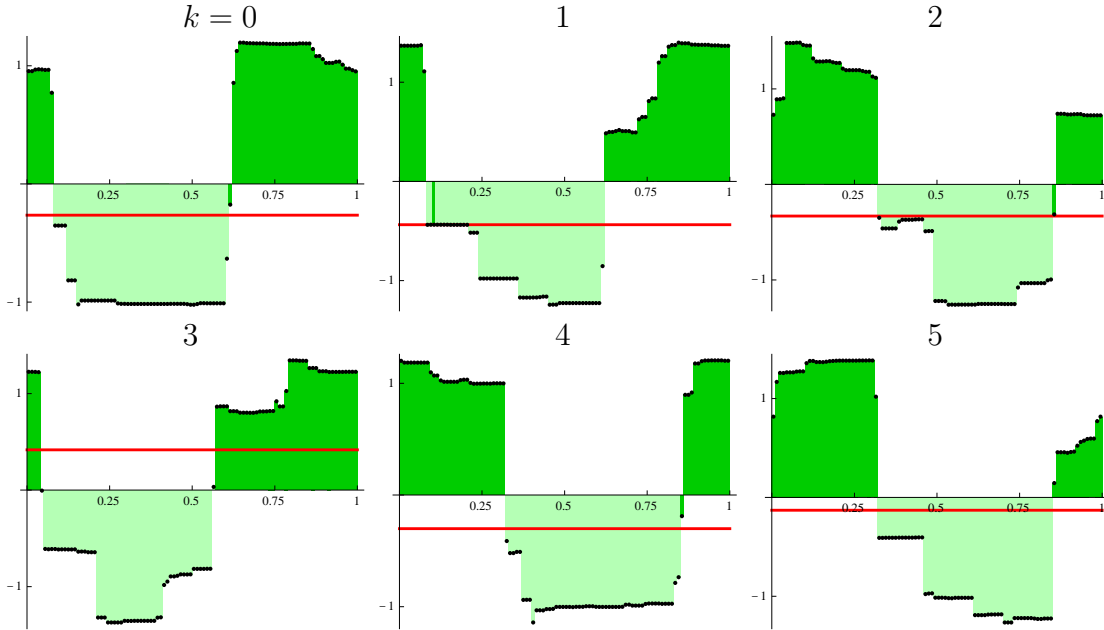


Figure 8: The Oseledets function approximations  $f_2^{(M,N)}(\sigma^k\omega)$  for  $M = 20, N = 10$ , and  $k = 0, \dots, 5$ , along with optimal thresholds, see Section 7.2.

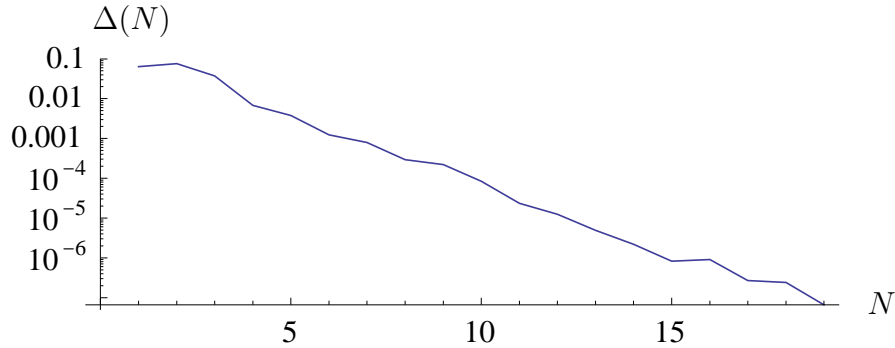


Figure 9: A graph showing  $\Delta(N)$  for  $N = 1, \dots, 19$ .

1 this distance should be small if the family  $W_2(\omega)$  is well approximated. A logarithmic plot of  $\Delta(N)$  against  $N$ , see Figure 9, shows the fast convergence of  $w_2^{(2N,N)}(\omega)$  to an Oseledets subspace. In Section 7.2 we will see how to extract coherent sets from these functions.

## 5.5 Oseledets functions in a 2D continuous time nonautonomous system

We consider the following nonautonomous system on  $M = [0, 2\pi] \times [0, \pi]$ ,  $t \in \mathbb{R}^+$ :

$$\begin{aligned} \dot{x} &= c - A \sin(x - \nu t) \cos(y) \quad \text{mod } 2\pi \\ \dot{y} &= A \cos(x - \nu t) \sin(y) \end{aligned} \tag{22}$$

This equation describes a travelling wave in a stationary frame of reference with rigid boundaries at  $y = 0$  and  $y = \pi$ , where the normal flow vanishes [33, 39]. The streamfunction

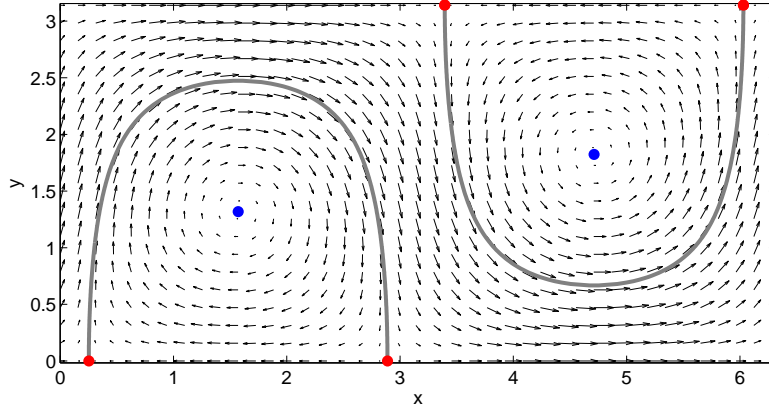


Figure 10: Vector fields in the comoving frame for the travelling wave flow (23), for  $A = 1.0$  and  $c = 0.5$ . The red dots are the hyperbolic fixed points that are connected by the heteroclinic loops. The blue dots are elliptic points in the centre of recirculation regions.

(Hamiltonian) of this system is given by

$$s(x, y, t) = -cy + A \sin(x - \nu t) \sin(y). \quad (23)$$

We set  $c = 0.5$ ,  $A = 1$ , and the phase speed to  $\nu = 0.25$ . The velocity field is  $2\pi$ -periodic in the  $x$ -direction, which allow us to study the flow on a cylinder. The velocity fields in a comoving frame for these parameters are shown in Figure 10. The closed recirculation regions adjacent to the walls ( $y = 0$  and  $y = \pi$ ) move in the positive  $x$ -direction and are separated from the jet flowing regime by the heteroclinic loops of fixed points, which are given below.

This model can be simplified to an autonomous system with a steady streamfunction in the comoving frame by setting  $X = x - \nu t$  and  $Y = y$ . The steady streamfunction is then given by  $S(X, Y, t) = -(c - \nu)Y + A \sin(X) \sin(Y)$ . Let  $X_s = \sin^{-1}((c - \nu)/A)$  and  $Y_s = \cos^{-1}((c - \nu)/A)$ . In the comoving frame, the recirculation region at the wall  $Y = 0$  contains an elliptic point  $q_1 = (\pi/2, Y_s)$  and is bounded by the heteroclinic loop of the hyperbolic fixed points  $p_1 = (X_s, 0)$  and  $p_2 = (\pi - X_s, 0)$ . Similarly, those elliptic and hyperbolic points at the wall  $Y = \pi$  are  $q_2 = (3\pi/2, \pi - Y_s)$ ,  $p_3 = (\pi + X_s, \pi)$ , and  $p_4 = (2\pi - X_s, \pi)$ , respectively, see Figure 10. One may observe that there is a continuous family of *invariant* sets in the comoving frame as any fixed level set of the streamfunction bounds an invariant set. In a stationary frame these elliptic and hyperbolic points (and their heteroclinic loops) are just translated in the  $x$ -direction. That is, any fixed level set of the time-dependent streamfunction (23) is a (time-dependent) invariant manifold. We note, however, that the recirculation regions are distinguished from the remainder of the cylinder as they are separated from the jet flowing region, which has a different dynamical fate. In the subsequent sections we will perturb this somewhat “degenerate” system to destroy the continuum of invariant sets in the comoving frame and produce a small number of almost-invariant sets (see Definition 5) in the comoving frame, or coherent sets in the stationary frame).

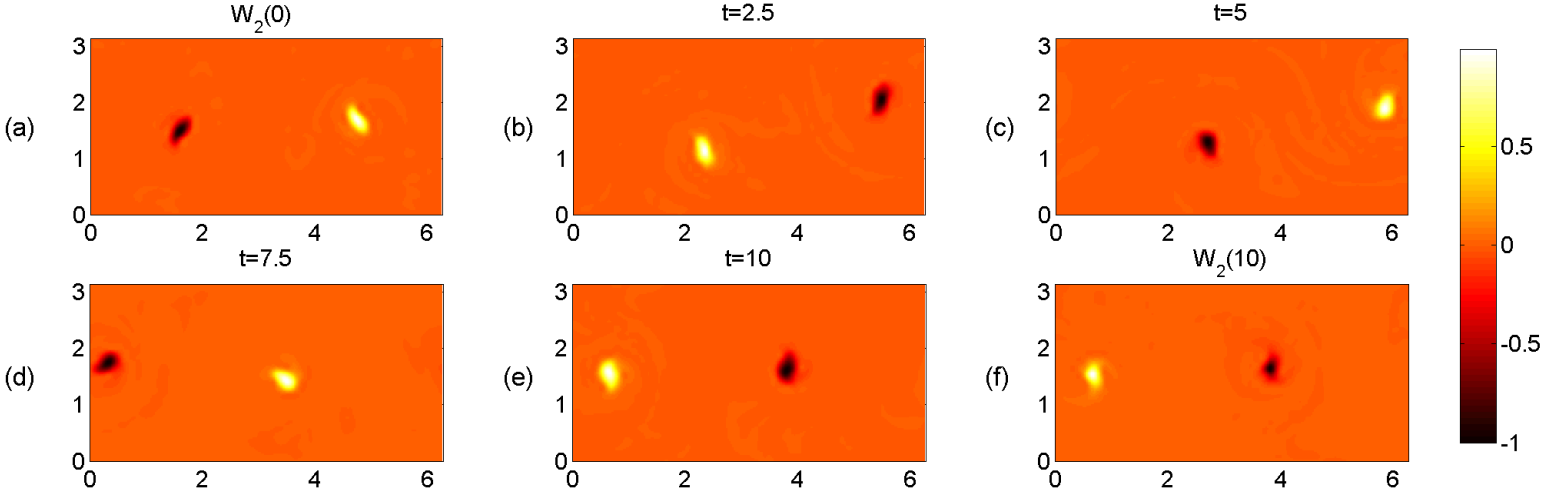


Figure 11: (a) Graph of approximate Oseledets function  $W_2^{(80,40)}(0)$  produced by Algorithm 4. (b)-(e) Pushforwards of  $W_2^{(80,40)}(0)$  via multiplication by  $P^{(\tau)}(0)$  for  $\tau = 2.5, 5, 7.5, 10$ . (f)  $W_2^{(80,40)}(10)$  produced independently by Algorithm 4; compare with (e)

### 5.5.1 A coherent family: Mixing case

We modify the travelling wave model in the previous section to allow mixing in the jet flowing region. We add a perturbation to the system in the following way:

$$\begin{aligned} \dot{x} &= c - A(t) \sin(x - \nu t) \cos(y) + \varepsilon G(g(x, y, t)) \sin(t/2) \\ \dot{y} &= a \cos(x) \sin(y). \end{aligned} \quad (24)$$

Here,  $A(t) = \sin(3t/2)/3+1$ ,  $G(z) := 1/(z^2 + 1)^2$  and the parameter function  $z = g(x, y, t) := A(t) \sin(x - \nu t) \sin(y) + y/2 - \pi/4$  vanishes at the level set of the streamfunction of the unperturbed flow at instantaneous time  $t=0$ , i.e.,  $s(x, y, 0) = \pi/4$ , which divides the phase space in half. Although this level set is not exactly at the middle of the jet regime of the perturbed system, the perturbation term is still large only in the vicinity of the middle of the jet regime but very small near the recirculation region. We set  $\varepsilon = 1$  as this value is sufficiently large to ensure no KAM tori remain in the jet regime, but sufficiently small to maintain islands originating from the nested periodic orbits around the elliptic points of the unperturbed system.

We applied Algorithm 3 with  $n = 7200$ ,  $M = 80$ ,  $N = 40$ ,  $t = 0$ , and Algorithm 4 for  $t = 0$  and  $t = 10$ . By using a relatively large number of test points per grid box ( $n = 7200$  points per box  $B_j$ ) we are able to flow for  $M = 80$  units of time and still well represent  $\phi(80, -40, B_j)$ . Figure 11 shows that the resulting Oseledets functions highlight the remaining islands in the perturbed time-dependent flow. We calculate the eigenvalues of  $(P^{(80)}(-40)^\top \circ P^{(80)}(-40))^{1/2}$ , where  $P^{(80)}(-40)$  is defined as in (20), and find the top three to be

$$L_1 \approx 1.0721, L_2 \approx 0.8818, L_3 \approx 0.8809.$$

By part 3 of Theorem 1 (bundle invariance of  $W_2(t)$ ) we should have  $P^{(10)}(0)W_2^{(80,40)}(0) \approx$

$W_2^{(80,40)}$  (10). This is demonstrated in Figure 11 by comparing subplots (e) and (f). In Section 7.3 we will see how to extract coherent sets from these Oseledets functions.

## 6 Invariant Sets, Almost-Invariant Sets, and Coherent Sets

We begin by briefly recounting some of the background relevant to almost-invariant sets. If  $\Phi$  (resp.  $\phi$ ) is autonomous, then  $\Omega$  (resp.  $\Xi$ ) consists of a single point, and we may write  $\Phi(-1, \omega, x) = \Phi(-1, x)$  (resp.  $\phi(-t, z, x) = \phi(-t, x)$ ).

**Definition 4.** In the autonomous setting, we call  $A$  an *invariant set* if  $\Phi(-1, A) = A$  (resp.  $\phi(-t, A) = A$  for all  $t \geq 0$ ).

The following definition generalises invariant sets to *almost-invariant sets*. In the continuous time case we define:

**Definition 5.** Let  $\mu$  be preserved by the autonomous flow  $\phi$ . We will say that a set  $A \subset M$  is  $\rho_0$ -almost-invariant over the interval  $[0, \tau]$  if

1.

$$\rho_{\mu, \tau}(A) := \frac{\mu(A \cap \phi(-s, A))}{\mu(A)} \geq \rho_0 \quad (25)$$

for all  $s \in [0, \tau]$ ,

2.  $A$  is connected.

If  $A \subset M$  is *almost-invariant* over the interval  $[0, \tau]$ , then for each  $s \in [0, \tau]$ , the probability (according to  $\mu$ ) of a trajectory leaving  $A$  at some time in  $[0, s]$ , and not returning to  $A$  at time  $s$  is relatively small. In the discrete time setting,  $\tau = 1$ , and the obvious changes are made in Definition 5. By convention we ask that  $A$  is connected; if  $A$  is not connected, we consider each connected component to be an almost-invariant set for suitable  $\rho_0$ .

We now begin to discuss the nonautonomous setting. The notion of an invariant set is extended to an *invariant family*.

**Definition 6.**

1. **Discrete time:** We will call a family of sets  $\{A_{\sigma^k \omega}\}$ ,  $A_{\sigma^k \omega} \subset M$ ,  $\omega \in \Omega$ ,  $k \in \mathbb{Z}$  an *invariant family* if  $\Phi(-k, \omega, A_\omega) = A_{\sigma^{-k} \omega}$  for all  $\omega \in \Omega$  and  $k \in \mathbb{Z}^+$ .

2. **Continuous time:** We will call a family of sets  $\{A_{\xi(t, z)}\}$ ,  $A_{\xi(t, z)} \subset M$ ,  $z \in \Xi$ ,  $t \in \mathbb{R}$  an *invariant family* if  $\phi(-t, z, A_z) = A_{\xi(-t, z)}$  for all  $z \in \Xi$  and  $t \in \mathbb{R}^+$ .

Motivated by a model of fluid flow, we imagine coherent sets as a family of *connected* sets with the property that the set  $A_\omega$  is *approximately* mapped onto  $A_{\sigma^k \omega}$  by  $k$  iterations of the cocycle from “time”  $\omega$ ; that is,  $\Phi(k, \omega, A_\omega) \approx A_{\sigma^k \omega}$ . The definition of coherent sets combines the properties of almost-invariant sets and an invariant family. As we now have a *family* of sets we require one more property beyond those of Definition 5, in addition to modifying the almost-invariance property. In the continuous time case we define:

**Definition 7.** Let  $\mu$  be preserved by a flow  $\phi$  and  $0 \leq \rho_0 \leq 1$ . Fix a  $z \in \Xi$ . We will say that a family  $\{A_{\xi(t,z)}\}_{t \geq 0}$ ,  $A_{\xi(t,z)} \subset M$ ,  $t \geq 0$  is a *family of  $\rho_0$ -coherent sets* over the interval  $[0, \tau]$  if:

1.

$$\rho_\mu(A_{\xi(t,z)}, A_{\xi(t+s,z)}) := \frac{\mu(A_{\xi(t,z)} \cap \phi(-s, \xi(t+s, z), A_{\xi(t+s,z)}))}{\mu(A_{\xi(t,z)})} \geq \rho_0, \quad (26)$$

for all  $s \in [0, \tau]$  and  $t \geq 0$ ,

2. Each  $A_{\xi(t,z)}$ ,  $t \geq 0$  is connected,

3.  $\mu(A_{\xi(t,z)}) = \mu(A_{\xi(t',z)})$  for all  $t, t' \geq 0$ ,

In discrete time, we replace (26) with

$$\rho_\mu(A_\omega) := \frac{\mu(A_\omega \cap \Phi(-1, \sigma\omega, A_{\sigma\omega}))}{\mu(A_\omega)} \geq \rho_0, \quad (27)$$

$\tau$  necessarily becomes 1, and we make the obvious changes to the other items in Definition 7.

We remark that by selecting some  $A \subset M$  of positive  $\mu$  measure and defining  $A_{\xi(t,z)} := \phi(t, z, A)$ ,  $t \geq 0$ , the family  $\{A_{\xi(t,z)}\}_{t \geq 0}$ , is a family of 1-coherent sets. Such a family is not of much dynamical interest, as there is nothing distinguishing this family from one constructed with another connected subset  $A' \subset M$ . We are not interested in these constructions of coherent sets, and in practice the numerical algorithm we present in the next section is unlikely to find such sets for chaotic systems.

## 7 Coherent sets from Oseledets functions

We wish to find a family of sets  $\{A_t\}_{t \geq 0}$  so that

$$\rho_\mu(A_t, A_{t+s}) := \frac{\mu(A_t \cap \phi(-s, t+s, A_{t+s}))}{\mu(A_t)} \quad (28)$$

is large for all  $t \geq 0$  and  $s \in [0, \tau]$ . We may rewrite the RHS of (28) as

$$\left( \int \chi_{A_t} \cdot \chi_{\phi(-s, A_{t+s})} d\mu \right) / \mu(A_t) = \left( \int \chi_{A_t} \cdot \chi_{A_{t+s}} \circ \phi(s, t) d\mu \right) / \mu(A_t) \quad (29)$$

$$= \left( \int \mathcal{P}_t^{(s)} \chi_{A_t} \cdot \chi_{A_{t+s}} d\mu \right) / \mu(A_t). \quad (30)$$

For (30) to be large we require  $\mathcal{P}_t^{(s)} \chi_{A_t} \approx \chi_{A_{t+s}}$ .

Let us now make a connection with the Oseledets functions  $f_2(t) = \sum_{i=1}^n w_{2,i}(t) \chi_{B_i}$  where  $w_2(t) \in W_2^{(M,N)}(t)$  obtained in Algorithm 4. In the following discussion, we scale  $f_2(t)$  so that  $\|f_2(t)\|_1 = 1$  for all  $t \geq 0$ . To convert the family of Oseledets functions into a family of coherent sets, we modify a heuristic due to [7] that has been successfully used in the autonomous setting. The heuristic is to set  $A_t = \{f_2(t) > 0\}$ ,  $t \geq 0$ . We show that  $\mathcal{P}_t^{(s)} f_2^+(t) - f_2^+(t+s)$  is small for moderate  $s$  and large  $\lambda_2$ ; we then heuristically infer that  $\mathcal{P}_t^{(s)} \chi_{A_t} \approx \chi_{A_{t+s}}$ .

**Proposition 3.** *Let  $\lambda_2 = \lim_{s \rightarrow \infty} (1/s) \log \|\mathcal{P}_t^{(s)} f_2(t)\| < 0$  be the second largest Lyapunov exponent from Theorem 1 and  $f_2(t) \in W_2(t)$  the corresponding Oseledets function, normalised so that  $\|f_2(t)\|_1 = 1$ . Given an  $\epsilon > 0$  there is an  $S \geq 0$  so that  $s \geq S$  implies  $\|\mathcal{P}_t^{(s)} f_2^+(t) - f_2^+(t+s)\|_1 \leq (1 - e^{(\lambda_2 - \epsilon)s})/2$ .*

*Proof.* Given  $\epsilon > 0$  we know that there exists  $S \geq 0$  such that for all  $s \geq S$  one has  $e^{\lambda_2 - \epsilon} \leq \|\mathcal{P}_t^{(s)} f_2(t)\|^{1/s} \leq 1$ . Since  $\mathcal{P}_t^{(s)} f_2(t) = (\mathcal{P}_t^{(s)} f_2(t))^+ - (\mathcal{P}_t^{(s)} f_2(t))^-$  and  $\int \mathcal{P}_t^{(s)} f_2(t) dm = 0$ , one has  $\|\mathcal{P}_t^{(s)} f_2(t)\|_1 = \int (\mathcal{P}_t^{(s)} f_2(t))^+ + (\mathcal{P}_t^{(s)} f_2(t))^- dm = 2 \int (\mathcal{P}_t^{(s)} f_2(t))^+ dm$ . Thus  $\int (\mathcal{P}_t^{(s)} f_2(t))^+ dm \geq e^{(\lambda_2 - \epsilon)s}/2$ . Since  $(\mathcal{P}_t^{(s)} f_2(t))^+ \leq \mathcal{P}_t^{(s)} f_2^+(t)$ , one has  $\|\mathcal{P}_t^{(s)} f_2^+(t) - (\mathcal{P}_t^{(s)} f_2(t))^+\| = \int \mathcal{P}_t^{(s)} f_2^+(t) - (\mathcal{P}_t^{(s)} f_2(t))^+ dm$ . As  $\|f_2(t)\| = 1$  and  $\int f_2(t) = 0$ , we have  $\int f_2^+(t) dm = 1/2$  and since  $\mathcal{P}_t^{(s)}$  preserves integrals,  $\int \mathcal{P}_t^{(s)} f_2^+(t) dm = 1/2$ . Thus,  $\int \mathcal{P}_t^{(s)} f_2^+(t) - (\mathcal{P}_t^{(s)} f_2^+(t)) dm \leq (1 - e^{(\lambda_2 - \epsilon)s})/2$   $\square$

The preceding discussion heuristically addresses item 1. of Definition 7. Regarding item 2 of Definition 7, as we are extracting the sets  $A_t$  from the Oseledets functions  $f_2(t)$ , the connectivity of the sets will depend on the regularity of the Oseledets functions. This is a delicate question and relatively little can be said formally at present. In the autonomous case, roughly speaking, one expects smooth eigenfunctions for Perron-Frobenius operators of smooth expanding systems [27, 38], and eigendistributions (smooth in expanding directions, distributions in contracting directions) in uniformly hyperbolic settings [3]. These properties may carry over to the non-autonomous setting. If a small amount of noise is added by postmultiplying the Perron-Frobenius operator by a smoothing (eg. diffusion) operator, then the Oseledets functions must be smooth. This physical addition of a small amount of noise is one way to guarantee regularity of the Oseledets functions and connectivity of the associated coherent sets.

Finally we note that if  $\mu = m$  one has  $\int f_2(t)(x) d\mu(x) = 0$  and so we must have  $\mu(A_t) = 1/2$  for all  $t \geq 0$ . Thus, item 3. of Definition 7 is satisfied by the choice  $A_t = \{f_2(t) > 0\}$ . If  $\mu \neq m$ , then it may be necessary to further tweak the choice of the  $A_t$  to ensure that item 3. of Definition 7 is satisfied. This additional tweak is described in Algorithm 5.

## 7.1 A numerical algorithm

For each fixed time  $t \geq 0$ , we seek to approximate a pair of sets  $A_t$  and  $A_{t+\tau}$  for which

$$\rho_\mu(A_t, A_{t+\tau}) := \frac{\mu(A_t \cap \phi(-\tau, t + \tau, A_{t+\tau}))}{\mu(A_t)} \quad (31)$$

is maximal. The quantity  $\rho_\mu(A_t, A_{t+\tau})$  is simply the fraction of  $\mu$ -measure of  $A_t$  that is covered by a pullback of the set  $A_{t+\tau}$  over a duration of  $\tau$ . For maximal coherence, we wish to find pairs  $A_t, A_{t+\tau}$  that maximise  $\rho_\mu(A_t, A_{t+\tau})$ . We present a heuristic to find such a pair of sets based upon the vectors  $W^{(M,N)}(t)$  and  $W^{(M,N)}(t + \tau)$ . This heuristic is a modification of heuristics to determine maximal almost-invariant sets, see [17, 15, 20]. In the terminology of the prior discussion in §7, rather than setting  $A_t := \{f_2(t) > 0\}$ , we allow  $A_t := \{f_2(t) > c\}$  or  $A_t := \{f_2(t) < c\}$  for some  $c \in \mathbb{R}$  in the hope of finding  $A_t, A_{t+\tau}$  with an even greater value of  $\rho_\mu(A_t, A_{t+\tau})$ . This additional flexibility also permits a matching of  $\mu(A_t)$  and  $\mu(A_{t+\tau})$ .

**Algorithm 5** (To determine a pair of maximally coherent sets at times  $t, t + \tau$ ).

1. Determine  $W^{(M,N)}(t)$  and  $W^{(M,N)}(t + \tau)$  for some  $0 \leq t < t + \tau$  according to Algorithm 4.
2. Set  $\hat{A}_t^+(c) = \bigcup_{i:W^{(M,N)}(t)_{i,c} > c} B_i$  and  $\hat{A}_{t+\tau}^+(c) = \bigcup_{i:W^{(M,N)}(t+\tau)_{i,c} > c} B_i$ , restricting the values of  $c$  so that  $\mu(\hat{A}_t^+(c)), \mu(\hat{A}_{t+\tau}^+(c)) \leq 1/2$ . These are sets constructed from grid boxes whose corresponding entry in the  $W^{(M,N)}$  vectors is above a certain value.
3. Define  $\eta(c) = \operatorname{argmin}_{c' \in \mathbb{R}} |\mu(\hat{A}_t^+(c)) - \mu(\hat{A}_{t+\tau}^+(c'))|$ . Given a value of  $c$ ,  $\eta(c)$  determines the set  $\hat{A}_{t+\tau}^+(\eta(c))$  that best matches the  $\mu$ -measure of  $\hat{A}_t^+(c)$ , as required by item 3 of Definition 7.
4. Set  $c^* = \operatorname{argmax}_{c \in \mathbb{R}} \rho_\mu(\hat{A}_t^+(c), \hat{A}_{t+\tau}^+(\eta(c)))$ . The value of  $c^*$  is selected to maximise the coherence.
5. Define  $A_t := \hat{A}_t^+(c^*)$  and  $A_{t+\tau} := \hat{A}_{t+\tau}^+(\eta(c^*))$ .

**Remark 7.**

1. One can repeat Algorithm 5, replacing  $\hat{A}_t^+(c)$  and  $\hat{A}_{t+\tau}^+(c)$  with  $\hat{A}_t^-(c) = \bigcup_{i:W^{(M,N)}(t)_{i,c} < c} B_i$  and  $\hat{A}_{t+\tau}^-(c) = \bigcup_{i:W^{(M,N)}(t+\tau)_{i,c} < c} B_i$  respectively. See [20] for further details.
2. Care should be taken regarding the sign of  $W^{(M,N)}(t)$  and  $W^{(M,N)}(t + \tau)$ . Visual inspection may be required in order to check that the vectors have the same “parity”.

## 7.2 Coherent Sets for a 1D discrete time nonautonomous system

We return to the map cocycle  $\Phi$  and Perron–Frobenius cocycle described in Example 1 and identify coherent sets. We use two methods: firstly, inspection of the composition of maps as perturbations of maps with invariant sets, and secondly using the general method of Algorithm 5.

The map cocycle  $\Phi$  is defined in terms of a map  $H_a$  which has an almost invariant set, and this gives rise to a family of coherent sets in the following way. Recall the definitions of the maps  $T_i$ ,  $i = 1, \dots, 4$  and shift space  $\Omega$  determined by the adjacency matrix  $B$ . The maps  $T_i$  have the property that if  $B_{i,j} = 1$ , then any inner  $R$  factors cancel in  $T_j \circ T_i$ . More generally, for any  $\omega \in \Omega$ , we have cancellation of all intermediate  $R$  factors:

$$\Phi(k, \omega, \cdot) = R^s \circ H_{a_{(\sigma^{k-1}\omega)_0}} \circ \dots \circ H_{a_{\omega_0}} \circ R^{-t}, \quad (32)$$

where  $s, t \in \{0, 1\}$  are given by

$$s(\omega, k) = \begin{cases} 0, & \omega_{k-1} \text{ odd,} \\ 1, & \omega_{k-1} \text{ even,} \end{cases} \quad \text{and} \quad t(\omega, k) = \begin{cases} 0, & \omega_0 \leq 2 \\ 1, & \omega_0 > 2. \end{cases}$$

For the map  $H_0$ , the interval  $[0, 0.5]$  is invariant. Moreover,  $[0, 0.5]$  is almost invariant for  $H_a$  with  $\rho_\mu([0, 0.5]) = 1 - 2a$ . By (32), we if we set

$$A_{\sigma^k \omega} = R^{s(\omega, k)}([0, 0.5]), \quad \text{for each } k \in \mathbb{N}, \quad (33)$$

then

$$\rho_\mu(A_{\sigma^k\omega}, A_{\sigma^{k+1}\omega}) = 1 - 2a_{\omega_k}.$$

Thus  $\mathcal{A} := \{A_{\sigma^k\omega}\}_{k \in \mathbb{N}}$  is a family of  $\rho_0$ -coherent sets with  $\rho_0 = 1 - 2 \max\{a_1, \dots, a_4\} = 0.843$ . In the same way, the invariant set  $[0.5, 1]$  of  $H_0$  leads to a family  $\{R^{s(\omega, k)}([0.5, 1])\}_{k \in \mathbb{N}}$  of  $\rho_0$ -coherent sets with the same  $\rho_0$ .

In order to demonstrate the methods of this article, we now show how Algorithm 5 can be used. We may use the Oseledets subspaces computed in Section 5.4 to find a family of coherent sets. First we apply Algorithm 5 to find a coherent set for the time step  $k = 0$  to  $k = 1$ . We calculate  $\rho_\mu(\hat{A}_0^+(c), \hat{A}_1^+(c))$  as  $c$  varies over the elements of the vector  $f_2^{(20,10)}(\omega)$ ; see Figure 12 (left). The maximum value of  $\rho_\mu(\hat{A}_0^+(c), \hat{A}_1^+(\eta(c)))$  is 0.890. The set  $A_\omega$  is found to be the interval  $[0.11, 0.58]$  of length  $\mu(A_\omega) = 0.47$ ; see Figure 12 (right).

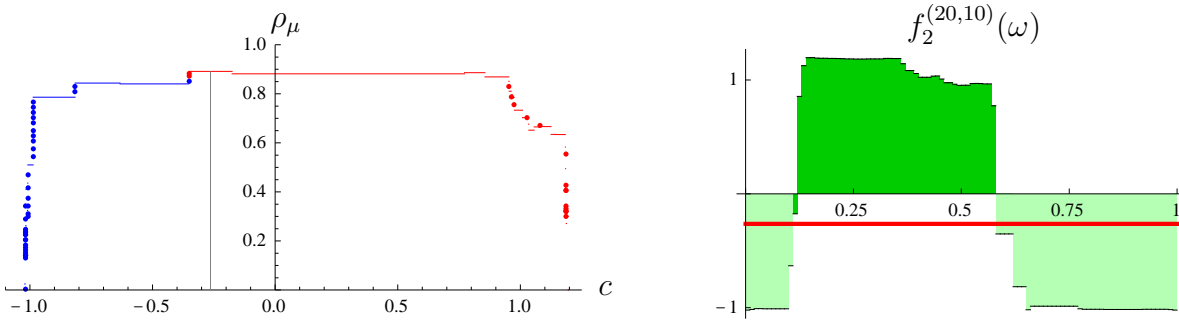


Figure 12: (left): The function  $\rho_\mu(\hat{A}_0^+(c), \hat{A}_1^+(\eta(c)))$  takes its maximum on the interval  $(-0.352, -0.176)$  and so we take the midpoint  $c^* = -0.264$  as the optimal threshold. (right): Taking this optimal threshold (shown in red) for the eigenvector  $f_2^{(20,10)}(\omega)$  identifies the coherent set  $A_\omega = [0.11, 0.58]$  (shown in dark orange).

We note that the set  $A_\omega$  found by Algorithm 5 is *not* the same as the  $A_\omega$  produced by the intuitive construction (33). In the latter case,  $A_\omega = [0, 1/2]$ ,  $A_{\sigma\omega} = [0, 1/2]$ , and  $\rho_\mu(A_\omega, A_{\sigma\omega}) = 1 - 2a_{\omega_0} = 1 - 2a_1 = 1 - \pi/20 \approx 0.843$ , significantly lower than the value of 0.890 found using Algorithm 5.

We may extend Algorithm 5 in order to find a sequence of coherent sets  $\{A_{\sigma^i\omega}\}_{i=0}^K$ . Since we require the measure of a sequence of coherent sets to be constant, we seek to maximize the mean value of  $\rho_\mu$  over a given time range as we vary the measure of the sets.

**Algorithm 6** (To determine a sequence of maximally coherent sets over a range of times  $t, \dots, t + K$ ).

1. Follow steps 1.-3. of Algorithm 5 for each  $k = 0, \dots, K - 1$  using  $\tau = 1$  to obtain sets  $\hat{A}_{t+k}^+(c)$ .
2. Let  $c_k(\ell) := \operatorname{argmin}_{c \in \mathbb{R}} |\mu(\hat{A}_{t+k}^+(c)) - \ell|$ .
3. Compute  $\ell^* := \operatorname{argmax}_{\ell \in (0, 0.5]} \frac{1}{K} \sum_{k=0}^{K-1} \rho_\mu(\hat{A}_{t+k}^+(c_k(\ell)), \hat{A}_{t+k+1}^+(c_{k+1}(\ell)))$ .

4. For  $k = 0, \dots, K - 1$ , define  $A_{t+k} := \hat{A}_{t+k}^+(c_k(\ell^*))$ .

To demonstrate Algorithm 6, we use the approximate Oseledets functions  $f_2(\sigma^k\omega)$ ,  $k = 0, \dots, 5$ , to find a sequence of six coherent sets  $\{A_{\sigma^k\omega}\}_{k=0}^5$  for the map cocycle  $\Phi$ . Plotting  $\frac{1}{6} \sum_{k=0}^5 \rho_\mu \left( \hat{A}_{\sigma^k\omega}^\pm(c_k(\ell)), \hat{A}_{\sigma^{k+1}\omega}^\pm(c_{k+1}(\ell)) \right)$  against  $\ell$  (see Figure 13), we find a unique maximum of 0.891, which occurs at  $\ell^* = 0.47$ .

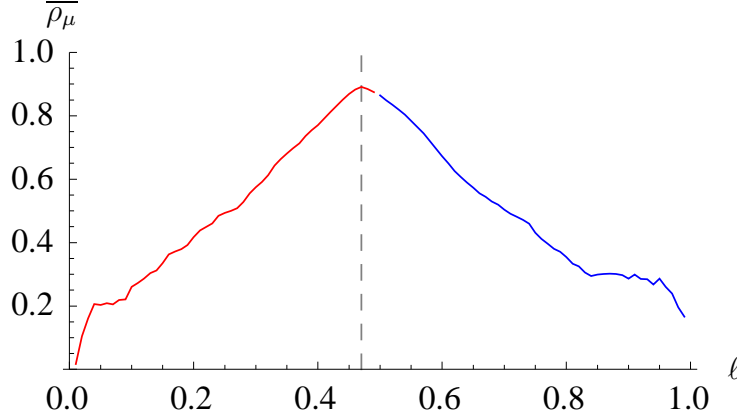


Figure 13: The graph of  $\bar{\rho}_\mu := \frac{1}{6} \sum_{k=0}^5 \rho_\mu \left( \hat{A}_{\sigma^k\omega}^\pm(c_k(\ell)), \hat{A}_{\sigma^{k+1}\omega}^\pm(c_{k+1}(\ell)) \right)$  against  $\ell$ , where we take  $\hat{A}_{\sigma^k\omega}^+(c_k(\ell))$  for  $\ell \le 0.5$  and  $\hat{A}_{\sigma^k\omega}^-(c_k(\ell))$  otherwise. The maximum 0.891 occurs at  $\ell^* = 0.47$ . The red section of the curve corresponds to  $\hat{A}_{\sigma^k\omega}^+(c_k(\ell))$  and the blue section to  $\hat{A}_{\sigma^k\omega}^-(c_k(\ell))$ .

Figure 8 shows the graph of  $f_2^{(20,10)}(\sigma^k\omega)$  with the threshold  $c_k(\ell^*)$  for  $k = 0, \dots, 5$ , and in each case the set  $\hat{A}_{\sigma^k\omega}^+(c_k(\ell^*))$  is indicated by shading. Since coherent sets are required to be connected, we must find the interval closest to each  $\hat{A}_{\sigma^k\omega}^+(c_k(\ell^*))$ . For  $k = 0, 2, 3, 4, 5$  the set  $\hat{A}_{\sigma^k\omega}^+(c_k(\ell^*))$  is itself an interval and we set  $A_{\sigma^k\omega} = \hat{A}_{\sigma^k\omega}^+(c_k(\ell^*))$ . The set  $\hat{A}_{\sigma^1\omega}^+(c_1(\ell^*))$  has two components,  $[0.12, 0.58]$  and  $[0.60, 0.61]$ , and so we set  $A_{\sigma\omega} = [0.12, 0.59]$ . Table 1 lists the coherent sets  $A_{\sigma^k\omega}$  and the values of  $\rho_\mu(A_{\sigma^k\omega}, A_{\sigma^{k+1}\omega})$  for  $k = 0, \dots, 5$ .

$k$	0	1	2	3	4	5
$\omega_k$	1	2	3	2	4	3
$A_{\sigma^k\omega}$	$[0.11, 0.58]$	$[0.12, 0.59]$	$[0.35, 0.82]$	$[0.07, 0.54]$	$[0.35, 0.82]$	$[0.35, 0.82]$
$\rho_k$	0.89	0.87	0.87	0.96	0.90	0.87

Table 1: Coherent sets  $A_{\sigma^k\omega}$  and the values of  $\rho_\mu(A_{\sigma^k\omega}, A_{\sigma^{k+1}\omega})$  for  $k = 0, \dots, 5$ .

It is interesting to compare the locations of the coherent sets with their corresponding maps in the mapping cocycle, see Figure 14. As for the previously constructed family  $\{R^{s(\omega,k)}([0.5, 1])\}_{k \in \mathbb{N}}$ , the coherent sets alternate between two positions separated by a rotation of approximately 0.25. However, the mean value of  $\rho_\mu$  is greater for the sequence  $A_{\sigma^k\omega}$  constructed from Algorithm 6 since in each case the coherent set matches up well with local maxima and minima of the preceding map.

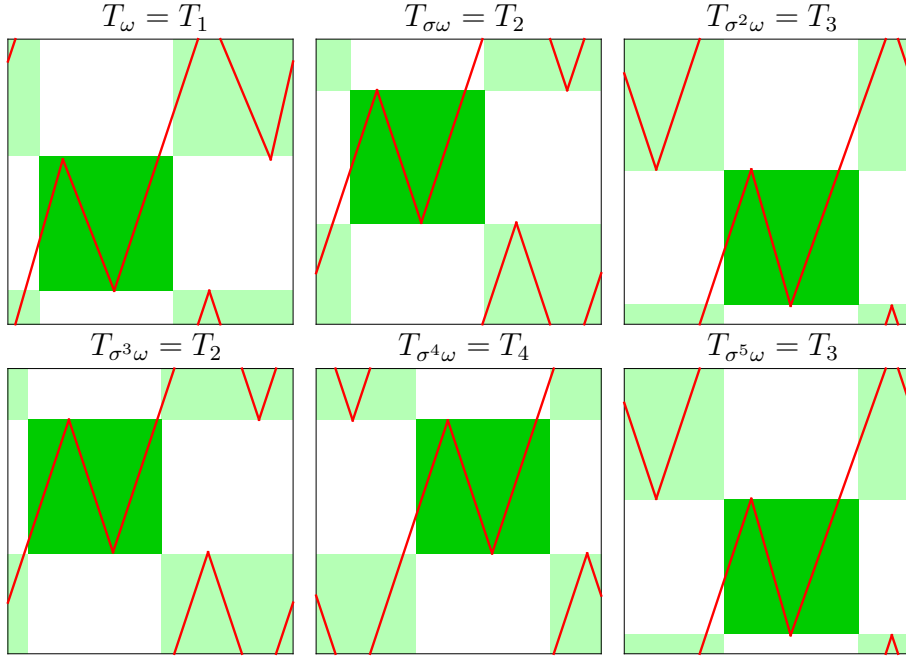


Figure 14: Graphs of  $T_{\sigma^k \omega}$  showing  $A_{\sigma^k \omega} \times A_{\sigma^{k+1} \omega}$  for  $k = 0, \dots, 5$ .

### 7.3 Coherent Sets in a 2D continuous time nonautonomous system

We apply Algorithm 5 to the Oseledets subspaces  $W^{(80,40)}(0)$  and  $W^{(80,40)}(10)$  calculated in Section 5.5.1 and displayed in Figure 11. The optimal coherent sets  $\hat{A}_0^+$  and  $\hat{A}_{10}^+$  for  $t = 0$ ,  $\tau = 10$  are obtained at the threshold values  $c^* = 0.1100$  and  $\eta(c^*) = 0.1263$ , which gives  $\rho_\mu(\hat{A}_0^+(c^*), \hat{A}_{10}^+(\eta(c^*))) = 0.8979$ , see Figure 15. For  $\hat{A}_0^-$  and  $\hat{A}_{10}^-$  the optimal threshold is at

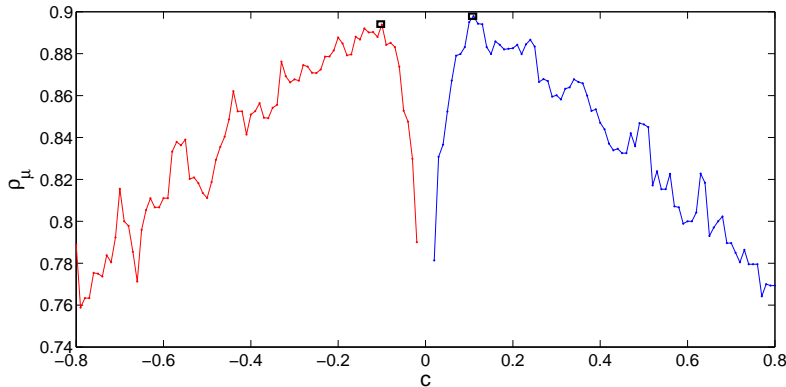


Figure 15: Thresholding curve  $\rho_\mu(\hat{A}_0^+(c), \hat{A}_{10}^+(\eta(c)))$  and  $(\rho_\mu(\hat{A}_0^-(c), \hat{A}_{10}^-(\eta(c))))$  are plotted in red and blue, respectively. The optimal threshold is marked with a rectangle.

$c^* = -0.1000$  and  $\eta(c^*) = -0.1160$  and  $\rho_\mu(\hat{A}_0^-(c^*), \hat{A}_{10}^-(\eta(c^*))) = 0.8939$ . The coherent sets at  $\hat{A}_0^+$  and  $\hat{A}_{10}^+$  and the images of sample points in  $\hat{A}_0^+$  are shown in Figure 16.

In Figure 16 we note that the light grey set on the left at  $t = 0$  flows approximately to the light grey set on the right at  $t = 10$ . Similarly for the dark grey set. This carrying

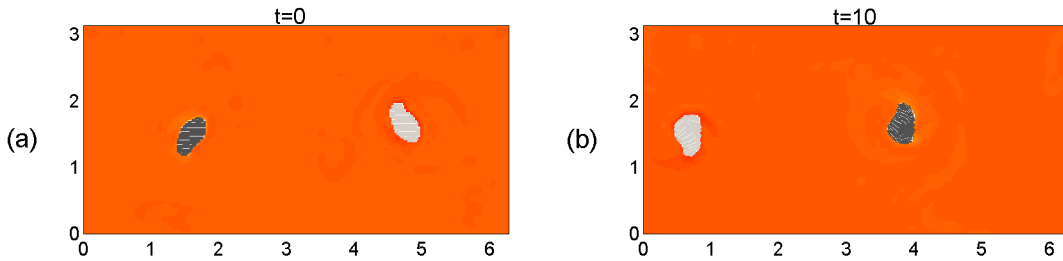


Figure 16: The coherent sets  $A_0^+$  and  $A_{10}^+$  (dark grey) and  $A_0^-$  and  $A_{10}^-$  (light grey) are identified by thresholding the Oseledets functions.

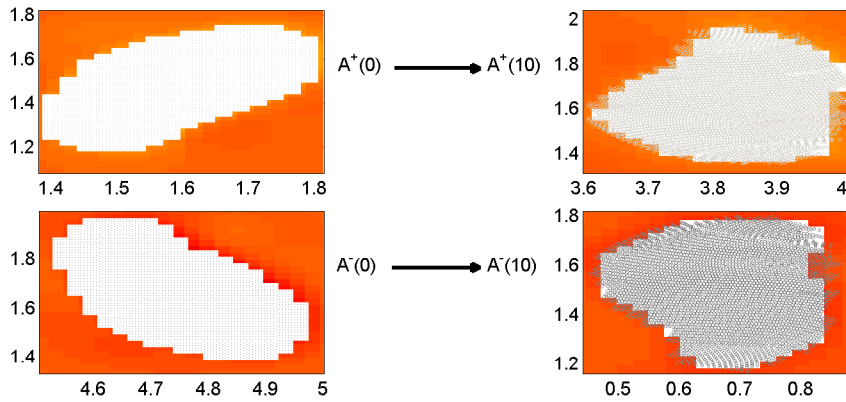


Figure 17: (left): Zooms of  $A^\pm(0)$ . (right): Overlays of  $\phi(10, 0, A^\pm(0))$  (dots) on  $A^\pm(10)$  (white), displaying the loss of mass over 10 time units duration from  $t = 0$ .

of the  $t = 0$  coherent sets to the  $t = 10$  coherent sets by the flow is only approximate, as  $\rho_\mu(\hat{A}_0^+(c^*), \hat{A}_{10}^+(\eta(c^*))) = 0.8979$  and  $\rho_\mu(\hat{A}_0^-(c^*), \hat{A}_{10}^-(\eta(c^*))) = 0.8939$ . Thus, we expect a loss of about 10% under the advection of the flow. Figure 17 zooms onto  $A^+(10)$  and  $A^-(10)$  to demonstrate this loss of mass. To make this loss even more apparent, we continue to flow forward for 50 time units. Figure 18 shows that the (black) coherent sets  $A_0^+$  and  $A_0^-$  do indeed disperse over time, however at a much slower rate than the arbitrarily chosen (grey) set. The coherent sets  $A_0^+, A_0^-$  are just single elements of a time parameterised family  $\{A_t^+, A_t^-\}_{t \geq 0}$  of coherent sets that at any given initial time describe those sets that will disperse most slowly over a duration of 10 time units.

## 8 Final Remarks

We have formulated a new mathematical and algorithmic approach for identifying and tracking coherent sets in nonautonomous systems. Our new approach generalises existing successful transfer operator methodologies that have been used in the autonomous setting. Our constructions address the question raised by [30] of how to study strange eigenmodes and persistent patterns observed in forced fluid flows in the general time-dependent situation. Future work will include applying these techniques to detect and track coherent regions in oceanic flow, extending significantly the flow times studied in [21] and [22].

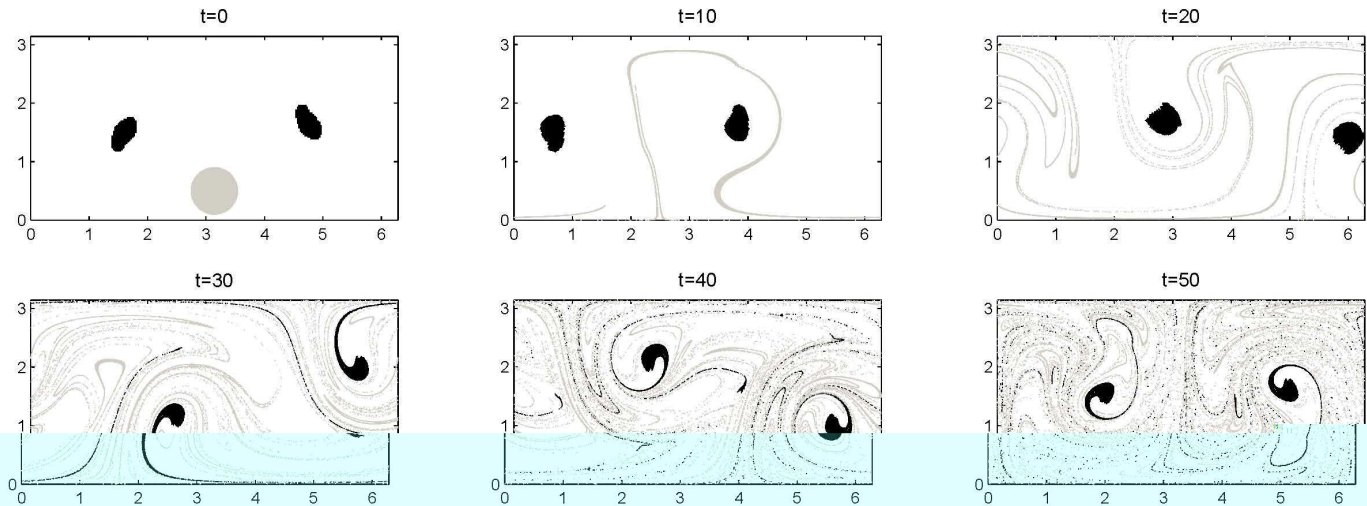


Figure 18: Trajectories of the perturbed system 24 for  $\varepsilon = 1$ . The black blobs are the coherent sets identified by our approach. The other (grey) blob is arbitrarily chosen to show they mix throughout non-coherent regions.

## References

- [1] H. Aref. The development of chaotic advection. *Physics of Fluids*, 14(4):1315–1325, 2002.
- [2] Ludwig Arnold. *Random Dynamical Systems*. Springer, Berlin, 1998.
- [3] Michael Blank, Gerhard Keller, and Carlangelo Liverani. Ruelle-Perron-Frobenius spectrum for Anosov maps. *Nonlinearity*, 15:1905–1973, 2002.
- [4] M. Dellnitz, O. Junge, W.S. Koon, F. Lekien, M.W. Lo, J.E. Marsden, K. Padberg, R. Preis, S.D. Ross, and B. Thiere. Transport in dynamical astronomy and multibody problems. *International Journal of Bifurcation and Chaos*, 15(3):699–727, 2005.
- [5] Michael Dellnitz, Gary Froyland, and Stefan Sertl. On the isolated spectrum of the Perron-Frobenius operator. *Nonlinearity*, 13:1171–1188, 2000.
- [6] Michael Dellnitz and Oliver Junge. Almost invariant sets in Chua’s circuit. *Int. J. Bif. and Chaos*, 7(11):2475–2485, 1997.
- [7] Michael Dellnitz and Oliver Junge. On the approximation of complicated dynamical behaviour. *SIAM Journal for Numerical Analysis*, 36(2):491–515, 1999.
- [8] P. Deuffhard, M. Dellnitz, O. Junge, and C. Schütte. Computation of essential molecular dynamics by subdivision techniques i: basic concept. In *In Computational Molecular Dynamics: Challenges, Methods, Ideas*, pages 98–115. Springer-Verlag, 1998.

- [9] P. Deuffhard, W. Huisinga, A. Fischer, and C. Schütte. Identification of almost invariant aggregates in nearly uncoupled Markov chains. *Linear Algebra and its Applications*, 315:39–59, 2000.
- [10] Jiu Ding and Aihui Zhou. Finite approximations of Frobenius-Perron operators. a solution of Ulam’s conjecture to multi-dimensional transformations. *Physica D*, 92(1–2):61–68, 1996.
- [11] N. Dunford and J. Schwarz. *Linear Operators, Part 1, General Theory*. Wiley, New York, 1988.
- [12] S. Ershov and A. Potapov. On the concept of stationary Lyapunov basis. *Physica D*, 118:167–198, 1998.
- [13] Gary Froyland. Finite approximation of Sinai-Bowen-Ruelle measures for Anosov systems in two dimensions. *Random and Computational Dynamics*, 3(4):251–263, 1995.
- [14] Gary Froyland. Ulam’s method for random interval maps. *Nonlinearity*, 12:1029–1052, 1999.
- [15] Gary Froyland. Statistically optimal almost-invariant sets. *Physica D*, 200:205–219, 2005.
- [16] Gary Froyland. Unwrapping eigenfunctions to discover the geometry of almost-invariant sets in hyperbolic maps. *Physica D*, 237(6):840–853, 2008.
- [17] Gary Froyland and Michael Dellnitz. Detecting and locating near-optimal almost-invariant sets and cycles. *SIAM J. Sci. Comput.*, 24(6):1839–1863, 2003.
- [18] Gary Froyland, Kevin Judd, and Alistair Mees. Estimation of Lyapunov exponents of dynamical systems using a spatial average. *Phys. Rev. E*, 51(4):2844–2855, 1995.
- [19] Gary Froyland, Simon Lloyd, and Anthony Quas. Coherent structures and Perron-Frobenius cocycles. Submitted, 2008.
- [20] Gary Froyland and Kathrin Padberg. Almost-invariant sets and invariant manifolds – connecting probabilistic and geometric descriptions of coherent structures in flows. Submitted, 2008.
- [21] Gary Froyland, Kathrin Padberg, Matthew H. England, and Anne Marie Treguier. Detection of coherent oceanic structures via transfer operators. *Physical Review Letters*, 98(22):224503, 2007.
- [22] Gary Froyland, Marcel Schwalb, Kathrin Padberg, and Michael Dellnitz. A transfer operator based numerical investigation of coherent structures in three-dimensional southern ocean circulation. In *Proceedings of the 2008 International Symposium on Nonlinear Theory and Applications*, Budapest, 2008.
- [23] F. Ginelli, P. Poggi, A. Turchi, H. Chaté, R. Livi, and A. Politi. Characterizing dynamics with covariant Lyapunov vectors. *Phys. Rev. Lett.*, 99, 2007.

- [24] G. Haller. Finding finite-time invariant manifolds in two-dimensional velocity fields. *Chaos*, 10:99–108, 2000.
- [25] George Haller. Distinguished material surfaces and coherent structures in three-dimensional fluid flows. *Physica D*, 149:248–277, 2001.
- [26] Tosio Kato. *Perturbation Theory for Linear Operators*. Springer-Verlag, Berlin, 1980.
- [27] Gerhard Keller. On the rate of convergence to equilibrium in one-dimensional systems. *Communications in Mathematical Physics*, 96:181–193, 1984.
- [28] Andrzej Lasota and Michael C. Mackey. *Probabilistic properties of deterministic systems*. Cambridge University Press, Cambridge, 1st edition, 1985.
- [29] Tien-Yien Li. Finite approximation for the Frobenius-Perron operator. A solution to Ulam’s conjecture. *Journal of Approximation Theory*, 17:177–186, 1976.
- [30] Weijiu Liu and George Haller. Strange eigenmodes and decay of variance in the mixing of diffusive tracers. *Physica D*, 188:1–39, 2004.
- [31] J. D. Meiss. Symplectic maps, variational principles, and transport. *Rev. Mod. Phys.*, 64(3):795–848, 1992.
- [32] Rua Murray. *Discrete approximation of invariant densities*. PhD thesis, University of Cambridge, 1997.
- [33] R.T. Pierrehumbert. Chaotic mixing of tracers and vorticity by modulated travelling Rossby waves. *Geophys. Astrophys. Fluid. Dyn.*, 58:285–320, 1991.
- [34] A. Pikovsky and O. Popovych. Persistent patterns in deterministic mixing flows. *Europhys. Lett.*, 61(5):625–631, 2003.
- [35] O.V. Popovych, A. Pikovsky, and B. Eckhardt. Abnormal mixing of passive scalars in chaotic flows. *Physical Review E*, 75:036308, 2007.
- [36] V. Rom-Kedar, A. Leonard, and S. Wiggins. An analytical study of transport, mixing and chaos in an unsteady vortical flow. *Journal of Fluid Mechanics*, 214:347–394, 1990.
- [37] V. Rom-Kedar and S. Wiggins. Transport in two-dimensional maps. *Archive for Rational Mechanics and Analysis*, 109:239–298, 1990.
- [38] David Ruelle. Characteristic exponents and invariant manifolds in Hilbert space. *Annals of Mathematics*, 115(2):243–290, 1982.
- [39] R.M. Samelson and S. Wiggins. *Lagrangian Transport in Geophysical Jets and Waves, The Dynamical System Approach*. Springer, United States of America, 2006.
- [40] Christof Schütte. *Conformational Dynamics: Modelling, Theory, Algorithm, and Application to Biomolecules*. ZIB, Berlin, 1999. Habilitation.

- [41] Christof Schütte, Wilhelm Huisinga, and Peter Deuffhard. Transfer operator approach to conformational dynamics in biomolecular systems. In Bernold Fiedler, editor, *Ergodic Theory, Analysis, and Efficient Simulation of Dynamical Systems*, pages 191–223. Springer, Berlin, 2001.
- [42] Shawn C. Shadden, Francois Lekien, and Jerrold E. Marsden. Definition and properties of Lagrangian coherent structures from finite-time Lyapunov exponents in two-dimensional aperiodic flows. *Physica D*, 212:271–304, 2005.
- [43] A. Trevison and F. Pancotti. Periodic orbits, Lyapunov vectors, and singular vectors in the lorenz system. *J. Atmos. Sci.*, 55:390399, 1998.
- [44] Warwick Tucker. The Lorenz attractor exists. *C. R. Acad. Sci. Paris, Série I*, pages 1197–1202, 1999.
- [45] S. Ulam. *Problems in Modern Mathematics*. Interscience, 1964.
- [46] S. Wiggins. *Chaotic Transport in Dynamical Systems*. Springer-Verlag, New York, NY, 1992.
- [47] S. Wiggins. The dynamical systems approach to Lagrangian transport in oceanic flows. *Annu. Rev. Fluid Mech.*, 37:295–328, 2005.